Use of Ground-Based Telescopes in Determining the Composition of the Surfaces of Solar System Objects [1]

Thomas B. McCord
Planetary Astronomy Laboratory
Department of Earth and Planetary Sciences
Massachusetts Institute of Technology
Cambridge, Massachusetts

John B. Adams
West Indies Laboratory
Fairleigh Dickinson University
St. Croix, Virgin Islands

The surfaces of solar system objects can be studied from Earth only by using electromagnetic radiation reflected and emitted from the surface materials. Of course one can leave the Earth's surface using spacecraft and study planetary surfaces more closely. Recent evidence suggests that the way that the surfaces of the solar system objects reflect solar radiation is controlled by the composition and mineralogy of the surface materials. The way sunlight is reflected from the surface as a function of wavelength, i.e., the spectral reflectance, is the most important property. This article reviews efforts by our laboratories to use ground-based optical telescope measurements to determine the composition of the surfaces of the solar system objects.

The spectral flux received at the Earth from a square kilometer of the lunar mare surface is plotted in figure 1. Here, flux in watts per square meter per micrometer is plotted against wavelength in micrometers. The radiation consists of two parts: (1) solar radiation passively reflected by the surface material, and (2) solar radiation which has been absorbed, converted to heat, and re-emitted as thermal radiation. The shapes of these two components of the spectral flux curve are similar for the surfaces of other solar system objects.

We are interested here only in the reflected solar component of the spectral flux available to the planetary astronomer. The property of interest is the spectral reflectance. It is defined as the fraction of sunlight incident on the surface which is reflected back into space from the object toward the observer.

Spectral reflectance is measured by us at the telescope using several instruments: mainly a dual-beam 24-filter photoelectric photometer, a two-dimensional integrating television-like imaging system, and a Michaelson interferometer spectrometer.

Measuring Spectral Reflectance

The function of interest in this discussion is the spectral reflectance $R(\lambda)$. It is defined as the fraction of incident radiation $F_{\odot}(\lambda)$ reflected back into space from the object $F_{obj}(\lambda)$ toward the observer.

$$R(\lambda) = F_{obj}(\lambda)/F_{\odot}(\lambda) \qquad (1)$$

[1]Massachusetts Institute of Technology, Planetary Astronomy Laboratory publication No. 102.

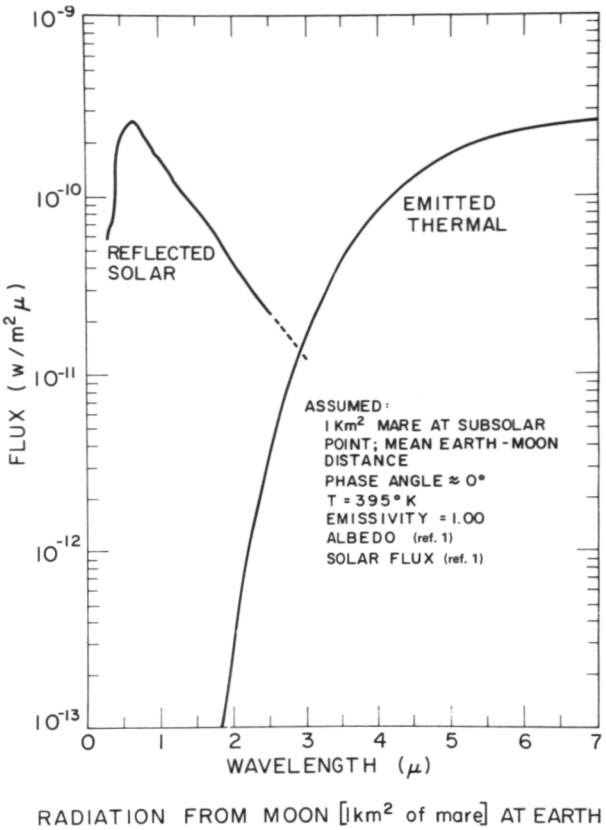

Figure 1.—*Radiation received from a 1-km square mare area, albedo 0.06 (ref. 1) at average Earth-Moon distance.*

We have ignored angular dependence and polarization, for they are of second-order importance to most of this discussion. We care mostly only about the wavelength dependence of the spectral reflectance and not so much about the albedo or absolute amount of reflected radiation.

Spectral reflectance is measured by us at the telescope using several instruments, mainly a filter photometer (ref. 2), a vidicon imaging system (refs. 3 and 4), and a Michaelson interferometer-spectrometer. The usual method of measurement is as follows:

1. The flux from the object of interest is measured.
2. At nearly the same time a nearby star is also observed.
3. The object/star flux ratio is formed, which should eliminate instrument response and atmospheric effects.
4. In previous studies the spectral flux of a series of these standard stars has been determined relative to a master standard star, α Lyrae, above the Earth's atmosphere (refs. 5 through 8).
5. Thus, the spectral flux received from the object is determined:

$$F_{obj} = \left(\frac{F_{obj}}{F_{ss}}\right)\left(\frac{F_{ss}}{F_{alyr}}\right) F_{alyr} \qquad (2)$$

F_{ss} = flux for standard star
F_{alyr} = flux for α Lyrae

6. Spectral reflectance is finally determined by using measurements and calculations of the spectral flux from the Sun above the Earth's atmosphere (ref. 9) (see equation (1)).

A more detailed discussion has been given by Chapman, McCord, and Johnson (ref. 10) and Elias (ref. 11).

Usually the spectral reflectance is displayed as a function scaled to unity at 0.56μm to eliminate albedo effects and concentrate on the spectral effects.

Theory

The spectral reflectance is of particular interest to us because there are several physical phenomena which cause selective absorption or sunlight. The theoretical basis for interpretation of visible and near-infrared spectra of minerals was established in a series of papers by Burns (refs. 12 and 13), White, and Keester (refs. 14 and 15) and Bancroft and Burns (ref. 16). These authors pioneered in the application of crystal-field theory to the interpretation of optical spectra of natural materials. White and Keester (ref. 14) and Adams and Filice (ref. 17) showed that diffuse reflectance spectra of powdered minerals retain the main spectral details that are observed in the transmission curves. Adams (ref. 18) presented evidence that absorption bands in the reflectance spec-

tra of planetary surfaces could be used to obtain information on remote mineralogy and petrology. Several authors have studied the reflectance properties of minerals and rocks from the point of view of interpreting remotely sensed spectra (refs. 19 through 27). Burns (ref. 13) provided a detailed discussion of the application of crystal-field theory to the study of minerals. Burns et al. (ref. 28), Bell et al. (ref. 29), and Gaffey and Burns (ref. 30) report on recent results in this rapidly expanding area of research where the spectra of single mineral grains are measured in polarized light.

Broad absorption bands appear at several wavelengths in the reflection spectrum. The best defined absorption bands are called electronic transition bands. They appear mostly at visible and near-infrared wavelengths. These are due to the photostimulated transition of d-shell electrons in transition element ions, principally iron. Less well defined, but often very strong, absorption features, appearing mostly at ultraviolet and visible wavelengths, are due to photostimulated transfers of electrons from one ion to another in the crystal lattice. These are called charge transfer bands.

Molecular vibrational bands also occur in the reflectance spectra of some minerals.

Variations in the wavelengths of the centers of the electronic absorption bands can be used to uniquely identify many mineral species. The energies of these absorptions are controlled by the kind of ions in the crystal lattice donating the electrons and by the electric field in which the ions are positioned. Therefore, the composition of the solid and the crystal structure of the solid control the wavelength position of the absorption bands.

The presence and wavelength position of the electronic absorption bands can be used to uniquely identify many mineral species. This is true regardless of whether one is studying silicates in the laboratory using an artificial light source or whether one is studying solar radiation reflected from the surface of the Moon using a ground-based optical telescope.

The Moon

It is appropriate to discuss the Moon first, for it is the object whose surface we know most about and for which we have the only ground-truth. A major portion of our effort in developing and applying the method or remote mineralogical analysis using reflection spectroscopy during the past 7 years has concerned the Moon. With the return of soil samples from eight lunar sites as a result of the U.S. and U.S.S.R. space programs, the opportunity for testing and expansion of the remote analysis is great. The experience gained in relating our ground-based telescope observations to the laboratory studies of lunar samples gives us confidence to proceed to the study of other solar system objects for which samples are not likely to be available in the near future.

Reflection spectra of small lunar regions with sufficient spectral resolution and intensity precision to define absorption features have only become available since 1968. The development of new instrumentation has allowed the determination of spectral reflectance curves for nearly 200 lunar regions of diameter 10 to 20 km, with photometric precision of about 1 percent (refs. 23 and 31).

A representative sample of these lunar spectral reflectance curves is shown in fig. 2, where reflectance as a function of wavelength is plotted. These curves represent the major morphologic units on the Moon: maria, uplands, and bright craters. Each curve is scaled to unity at 0.56μm. All of the curves measured are basically similar in shape. The spectral reflectance for all lunar areas increases toward longer wavelengths, and a shallow absorption band near 0.95μm occurs in all curves, but with varying depth and wavelength position. Beyond the spectral region shown here, into the infrared region to 2.5μm, the reflectivity continues to rise, and a very shallow, broad absorption band is evident near 2.0μm for many areas (ref. 32).

The absorption band in the lunar spectrum near 0.95μm is of direct mineralogical significance. There are small but important changes in its wavelength position from place

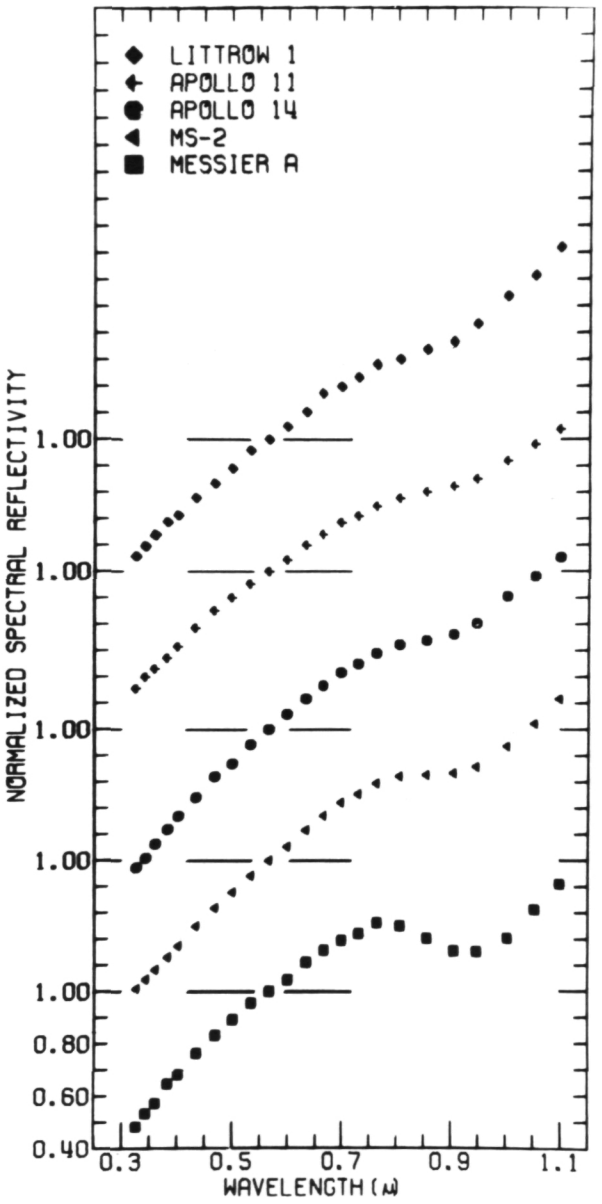

Figure 2.—*Spectral reflectivity of several 10- to 20-km-diameter areas of the lunar surface measured using ground-based telescopes.*

to place on the Moon, and the band depth varies greatly from strongest absorption at fresh bright crater sites to weakest absorption at "background" upland sites and at the very dark mare sites such as near the Apollo 17 site. From the laboratory studies of lunar and terrestrial metal-silicates and from theoretical analysis one would immediately interpret the absorption band in the lunar curves as indicating that pyroxene of pigeonite-augite composition is the major mafic mineral constituting the lunar mare surface material. This may not seem very profound after the return of samples from several U.S. and Soviet missions, but it was important when similar interpretations were made from less precise data before any lunar samples were available (refs. 2 and 18).

Changes in the position of the band near 0.95μm from place to place on the Moon are well documented (fig. 3). From the relationship between the wavelength position of this band and the composition of the pyroxenes causing it, it is clear that the average composition of the pyroxenes in the lunar soils varies from low calcium and iron at upland sites to high calcium and iron at mare sites. Deviations from this general rule do occur.

The slope of the spectral reflectance curve in the visible and near ultraviolet was a mystery until the first lunar samples were available. The slope is unlike that for normal pulverized silicates. The presence of glass rich in Fe^{2+}, Ti^{3+}, and Ti^{4+} ions and of the devitrified glasses rich in ilmenite and metallic iron are now known to be responsible for the unusual slope (refs. 33 through 37). An empirical relationship between the titanium content and curve slope of the reflection spectrum between 4000 and 5600 Å for mature ($\gtrsim$ 50-percent glassy soil aggregates) mare soils has been established (ref. 38). Figure 4 shows a plot of TiO_2 content versus this curve slope. Recent study of lunar samples indicates that the presence of titanium in the glasses is principally responsible for this relationship. The relation of titanium content to curve slope has allowed us to make a successful prediction of the composition of the Apollo 17 soils before they were returned to Earth (ref. 39). Other relationships between the composition of the surface material and the spectral reflectance curves, such as those involving exposure age, plagioclase content, and upland rock type, are presently being developed.

The telescope curves for all lunar areas are generally similar in shape; however,

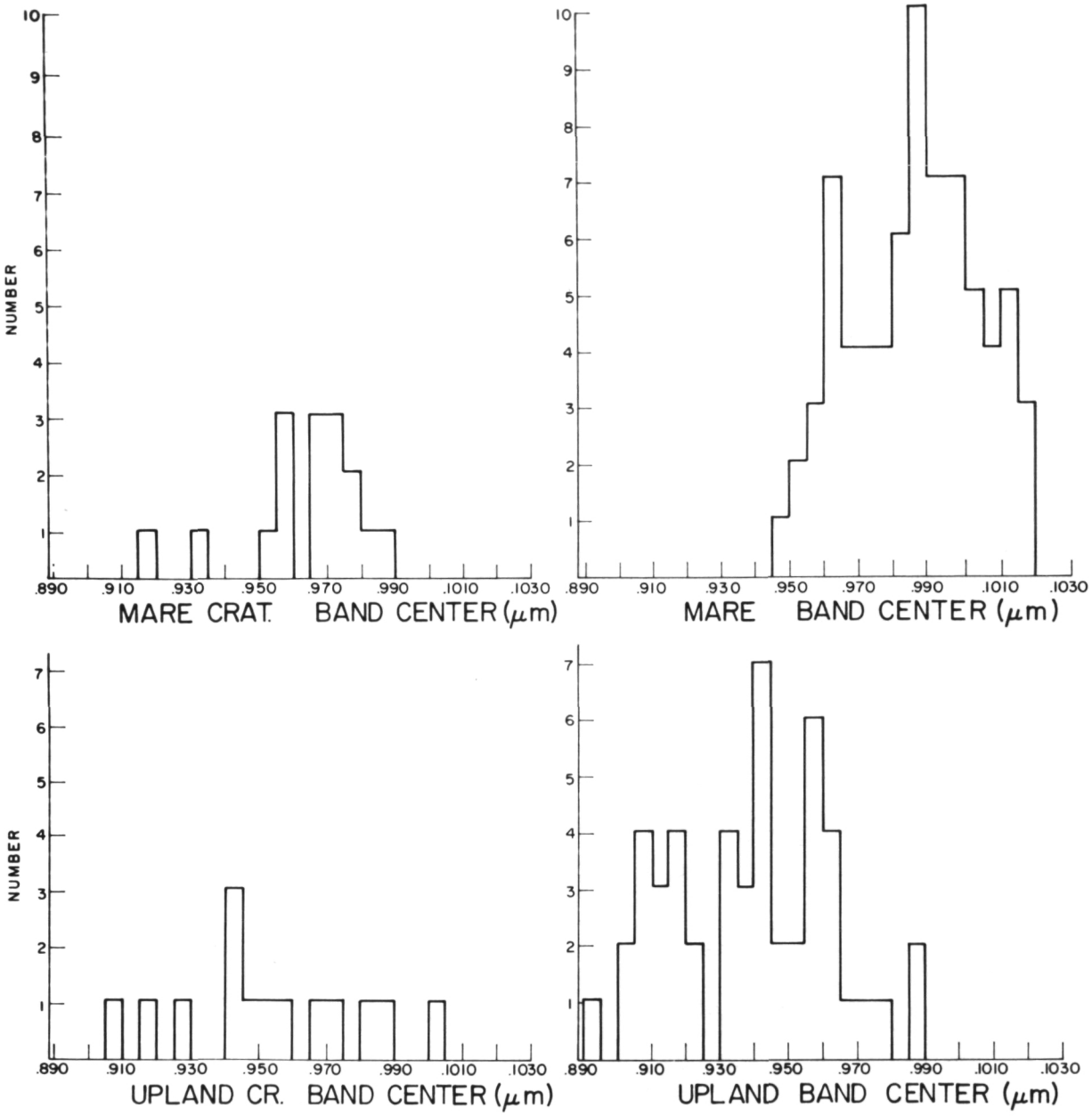

Figure 3.—*A frequency distribution of absorption band positions for each of the four major lunar morphologies. Telescope data are used.*

small but important differences exist that are best displayed by working with curve ratios. By dividing all spectral reflectance curves by the curve for a standard area on the Moon, one produces what we call relative reflectance curves, or curve ratios (ref. 3). We have analyzed more than 150 relative spectral curves for different areas of the Moon, and it becomes apparent that all the curves obtained can be arranged into four sets according to their shape. These four sets, we call them spectral types, are directly correlated with

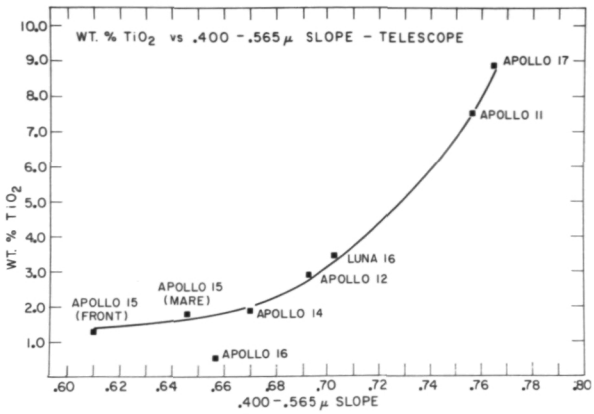

Figure 4.—*Precentage TiO_2 versus 0.400- to 0.565-μm slope of telescope curve. TiO_2 contents of telescopic areas an average of sampled soils.*

four morphologic units: mare, mare bright craters, uplands, and upland bright craters.

The relative curves, shown in figure 5a, illustrate the mare spectral type of curves. Notice the precision with which one can study the spectral properties of the lunar surface. The distance between each division on the plot axis is 2 percent in intensity. One can observe differences in these curves to well under 1 percent. Also note that there is not only one curve type, but a series of curves, indicating a series of mare materials. At the top of the series are the very dark "blue" maria such as are found in Mare Tranquillitatis. Near the middle of the series we have the brighter, "redder" mare such as Mare Serenitatis and the Apollo 12 site. At the bottom are the very "reddest" mare units such as Mare Frigoris. Some maria, especially imbrium, have patches of several types of material. Boundaries between different mare types seem to be accompanied by albedo boundaries, but all albedo boundaries are not color boundaries.

These relative plots are quite useful for quantitatively determining the compositional properties of the surface. For example, as shown in this figure, the mare relative curves exhibit a change in the slope of the curve in the blue and ultraviolet wavelengths. As stated before, this curve slope is related to titanium content in the mature soil. This

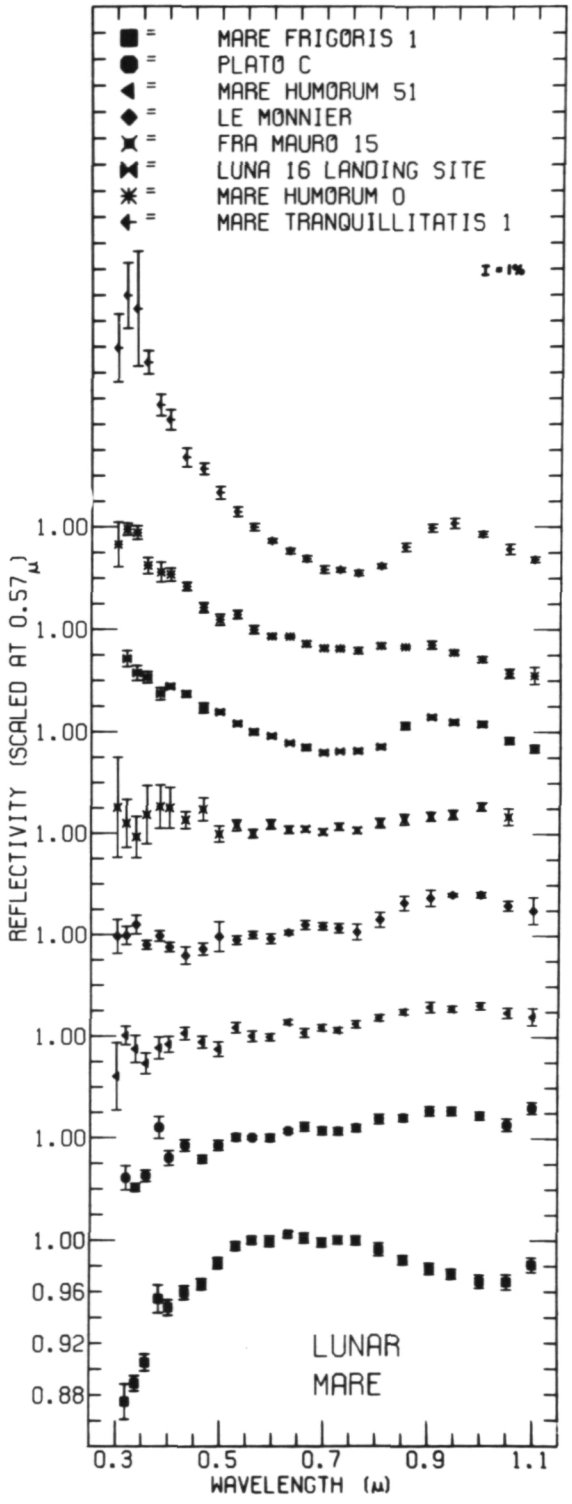

Figure 5a.—*Relative spectral reflectance for a series of mare areas.*

curve slope can be determined to better than 1 percent, and the titanium content can be determined to about 1 percent.

The next lunar spectral type is found in the uplands and is shown in figure 5b. In the uplands all curves are similar for the regions measured to date. The upland areas are defined here as almost any non-mare area other than bright craters. Notice as one progresses down the series of bright upland craters curves (fig. 5c) they become more and more like the background upland curves. This aging process, whereby bright upland crater material is changed into background upland material, can be explained using the Apollo samples (refs. 36 and 40).

The fourth distinct lunar surface spectral type is illustrated in figure 5d. Here are shown relative spectral curves for a series of bright mare craters. Notice that the absorption band near 0.95μm is much deeper than for any other lunar area, including up-

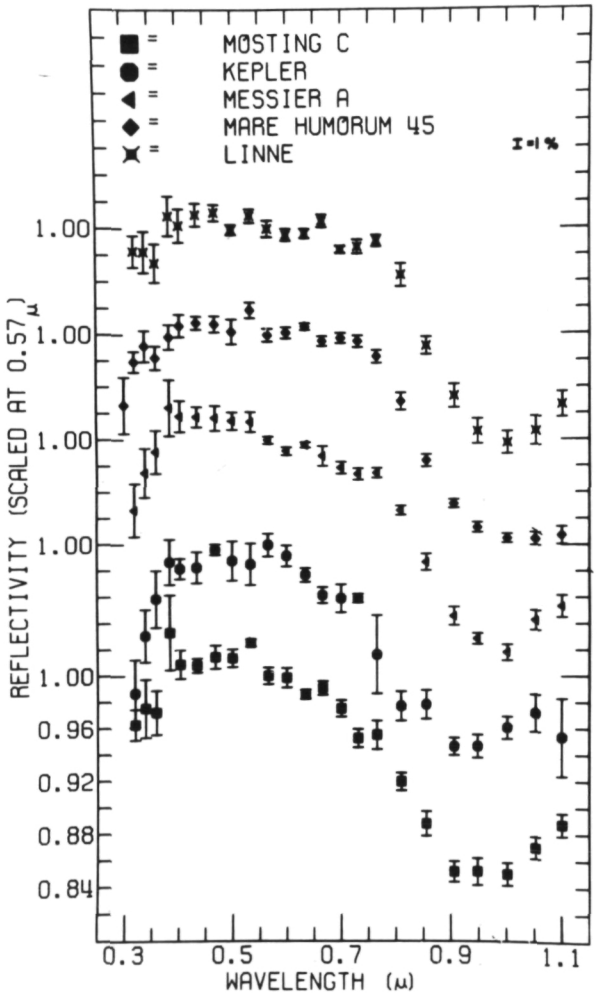

Figure 5c.—*Relative spectral reflectance for a series of upland areas.*

Figure 5b.—*Relative spectral reflectance for a series of mare bright craters.*

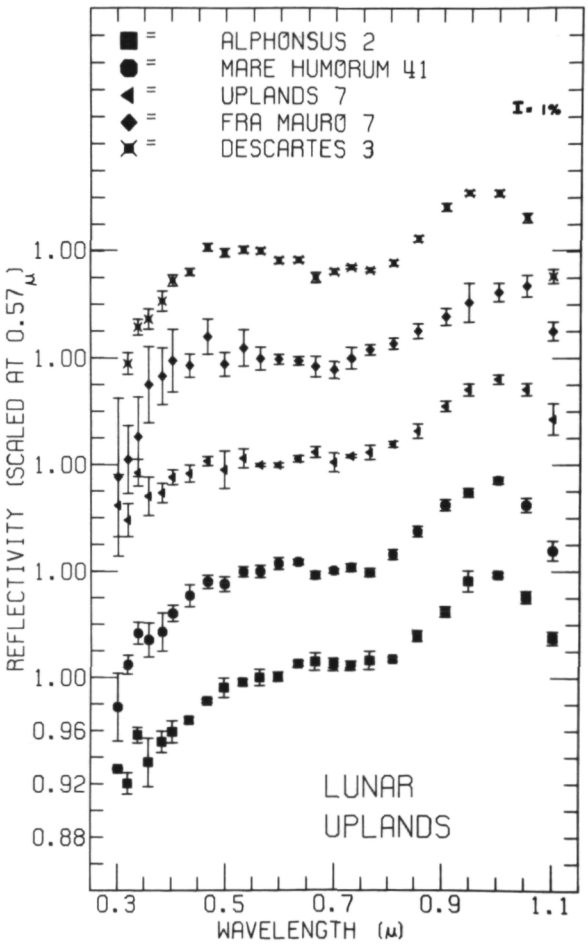

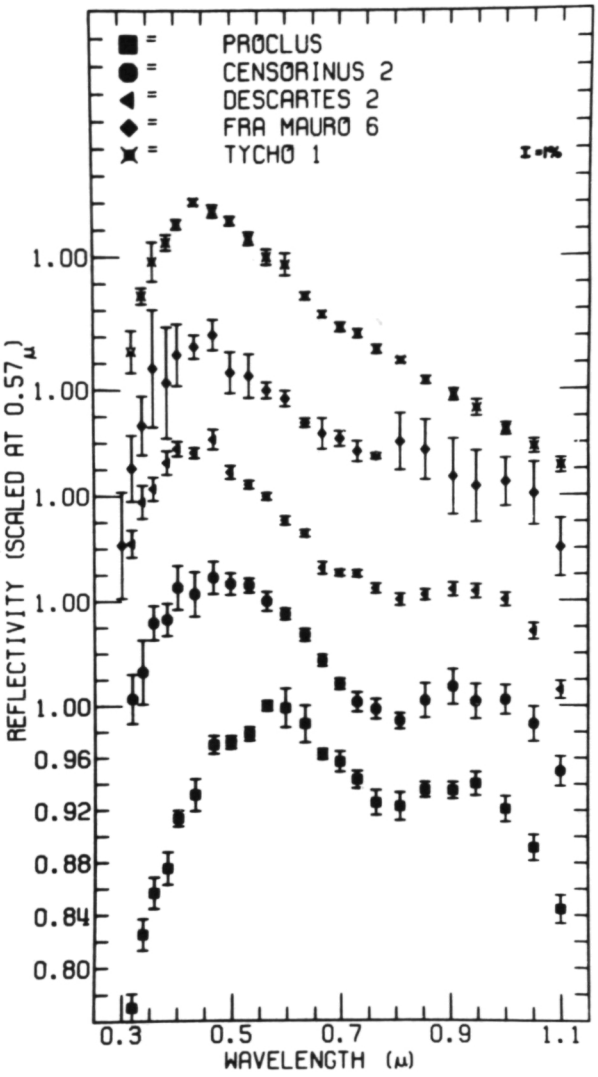

Figure 5d.—*Relative spectral reflectance for a series of upland bright craters.*

land bright craters. The mare bright craters also age, with their color as well as their brightness becoming nearer that of the background mare material.

It is of considerable interest that one can tell the difference between mare and upland materials even though the albedo may be the same, as say for bright craters. This technique has been used to show that Aristarchus is of the fresh upland crater type and Copernicus is of mature background upland material type, although they are formed in mare regions. These craters expose upland material that was excavated from beneath the mare fill. This result also suggests that the concept of darkening of craters with time, which has been used to judge crater ages, must be used with caution.

One of the first applications of the measurements of the lunar sample optical properties was to determine the accuracy of the telescope data. The laboratory-measured spectral reflectance of Apollo 11 soil samples obtained at each of the Apollo sites was compared with the spectral reflectance measured by telescope of 18-km-diameter areas containing the landing sites. The agreement between laboratory and telescope measurements is within a few percent (ref. 33). This same sort of comparison has been carried out for the later Apollo missions (fig. 6). The conclusions drawn from this comparison are (1) the telescope data are accurate to about 1 percent, and one is measuring the actual physical properties of the lunar surface; (2) the telescope measurements refer mainly to the lunar soil rather than to rocks or breccia. We have also been able to reproduce in the laboratory the relative spectral reflectance curves using Apollo soil samples.

The reason spectral types exist is revealed by analysis of the lunar samples. It was found that the Apollo 12 soil has spectral properties very similar to those of the telescopic standard area in Mare Serenitatis. The Mare Serenitatis curve is used as the denominator in the ratio called relative reflectance. Thus, lunar sample relative curves, using the Apollo 12 soil as a standard, should be directly comparable to the telescope curves using the Mare Serenitatis standard area (ref. 41). Figure 7 shows the laboratory relative spectral reflectivity curve for Apollo 11 soil overlayed on the telescope curve for the landing site area. Notice the change in the vertical axis scale from figure 6. The Apollo 11 soil clearly has a mare spectral type (fig. 5).

By crushing a mare rock from Apollo 12, the mare bright crater spectral type is reproduced (fig. 7). The powdered rock curve has been reduced in scale by a factor of four

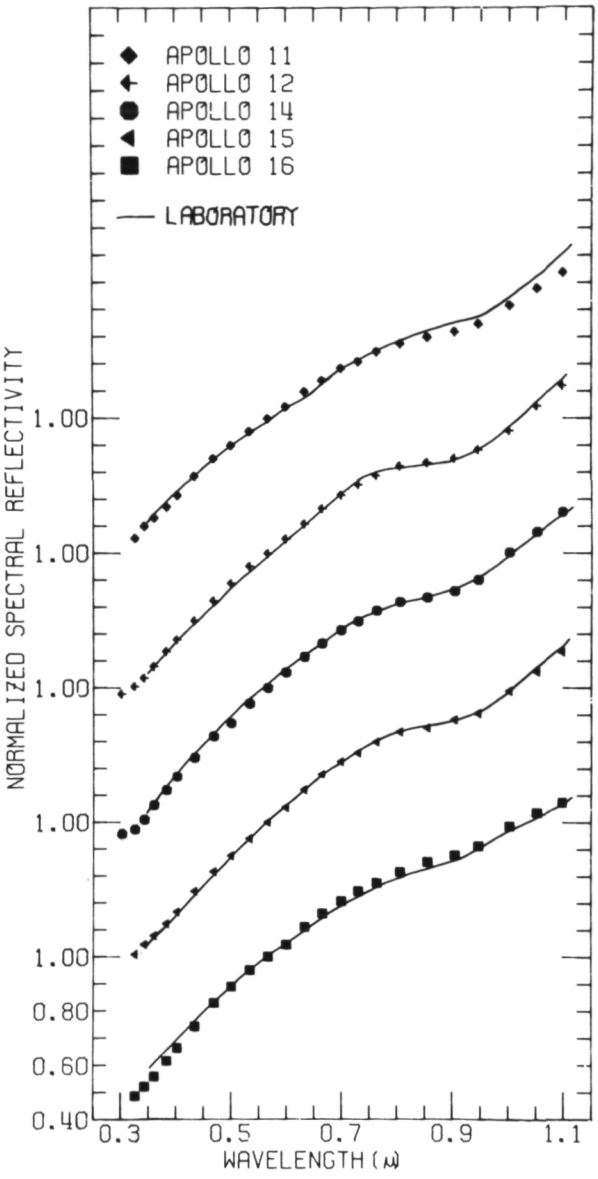

Figure 6.—*Spectral reflectivity of areas containing Apollo landing sites compared to laboratory measurements of soil returned from these sites.*

to better compare the shape of the two curves. The scale difference probably exists because the lunar soil even at a fresh mare crater is not entirely crystalline, but contains some glass.

The next comparison (fig. 7) is for Apollo 14 soil. Here the curve of the soil from the landing site matches the curve for the background upland spectral type. Finally, the upland bright crater curve is reproduced by a sample from Cone Crater, a bright fresh crater at the Apollo 14 site.

It is significant for remote analysis that the curves for lunar samples show the same subtle but important structures that also are seen in the telescope curves. Using the sample studies, the chemical and mineralogical properties that control the curve structure can be used to extend the compositional information gained at a few sites by direct sampling to the entire front surface of the Moon by ground-based remote observation.

Much of the work concerning the lunar telescope observations has been directed toward proving their accuracy and relevance to the properties of the surface material. Also, as discussed in other articles (e.g., ref. 42), considerable effort was expended to understand the optical properties of the lunar samples in order to better interpret the telescope curves.

We have also applied the telescope measurements to improve the understanding of the lunar surface. As discussed earlier in this article, telescopic curves were used to show that some mare bright craters had exposed upland material from beneath the mare, thereby defining a way of probing the depth of the maria and the composition of the subsurface material. Also, the titanium content and general rock type to be found at the Apollo 17 landing site was predicted correctly (ref. 39). The relationship of the regional geologic units at the Apollo 16 site (ref. 42) and the presence of Copernicus ray material in the Apollo 12 samples (ref. 40) were worked out partly by using telescopic data.

The current major effort to use the telescopic data is directed at mapping compositional units. Working with the spectral reflectance curves one learns to recognize several curve parameters, such as absorption band depth and curve slope in the blue, which are directly correlated with compositional information. It is obvious that one can map the spatial distribution of these curve parameters by imaging the Moon at certain

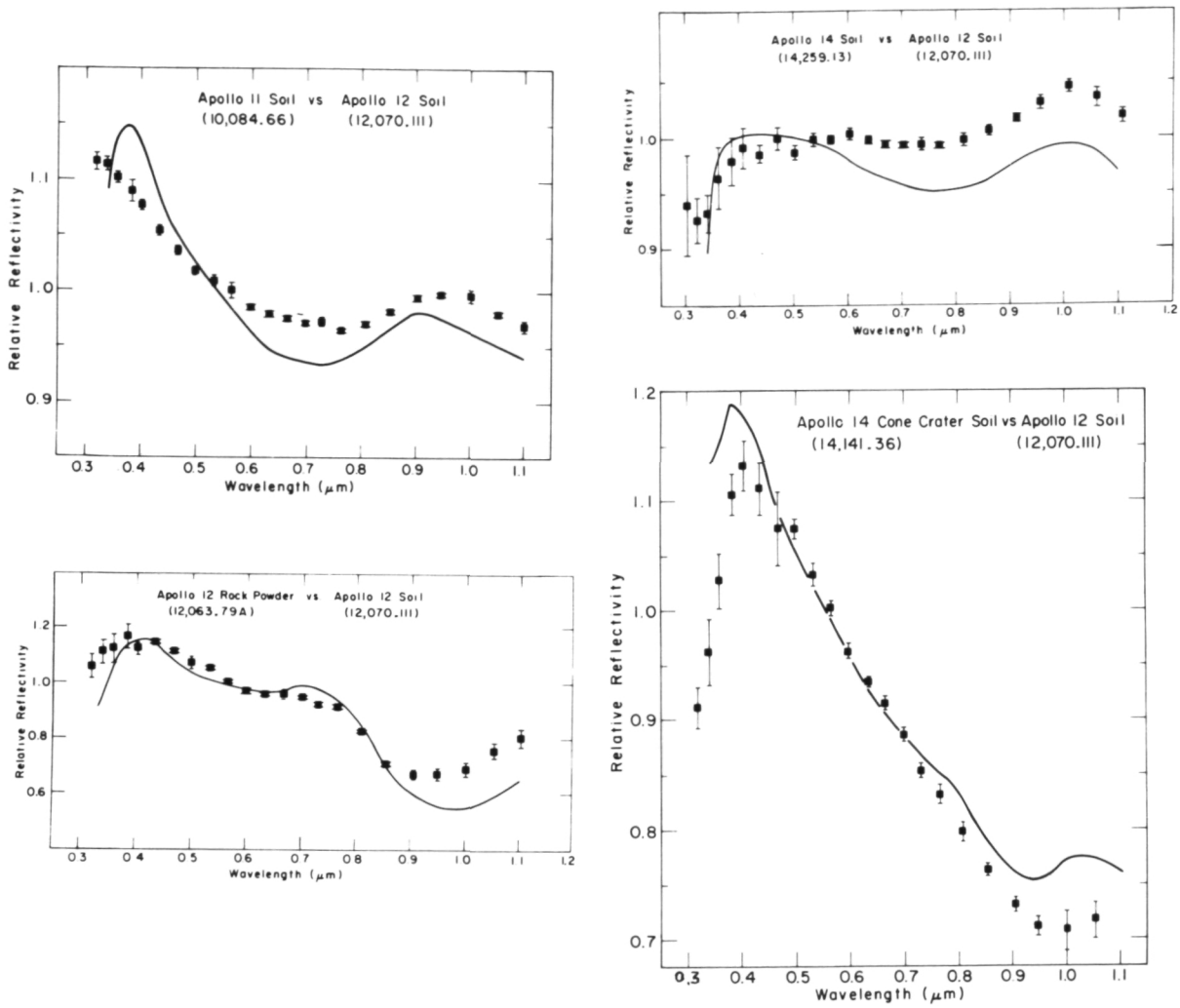

Figure 7.—*Comparison of relative spectral reflectivity curves measured in the laboratory and at the telescope.*

wavelengths and, thus, map the spatial distribution of the associated compositional properties. As an example, consider the relationship of curve slope between 0.40 and 0.56μm, with titanium content in mature mare soils. This curve slope can be mapped by dividing images of a lunar area made at the two wavelengths and producing an image of the ratio. Because the change in spectral properties is small, i.e., on the order of 1 to 10 percent, it is necessary to map these spectral parameters with high photometric precision in order to obtain useful compositional maps. In order to do this, we have developed a special imaging system (refs. 3 and 4) that uses a silicon diode array vidicon tube. This television-like system integrates the optical image the telescope presents to it much as a photographic plate does. When sufficient signal has been integrated on the detector, the two-dimensional detector is read out in a single-frame mode to present to the observer a highly photometrically precise image of, say, an area of the Moon. The image is recorded in digital form in order to be computer processed.

Figure 8a is an example of the application of this technique for the southeast Mare

Serenitatis region of the Moon (ref. 39). This color difference image is essentially a map of titanium content in the mare region to a precision of about 1 percent TiO_2. The Apollo 17 landing site is located in the Taurus-Littrow Valley shown in this figure. This map was produced by obtaining two images of this area of the Moon, using the vidicon imaging system. One image was made at 4000 Å and the other was made at 5600 Å. These digital images were calibrated in the computer, and then the calibrated images were divided: the 4000 Å image divided by the 5600 Å image, point by point, to produce an array of numbers which is a measure of the ratio of these two images. This ratio array, or ratio image, was then converted to a photographic image using a cathode ray tube to write on photographic film.

The result is seen in the figure. Here brighter means higher in titanium content. The amplitude of the titanium content variations in the image is only a few percent. This ratio image has been contrast enhanced to

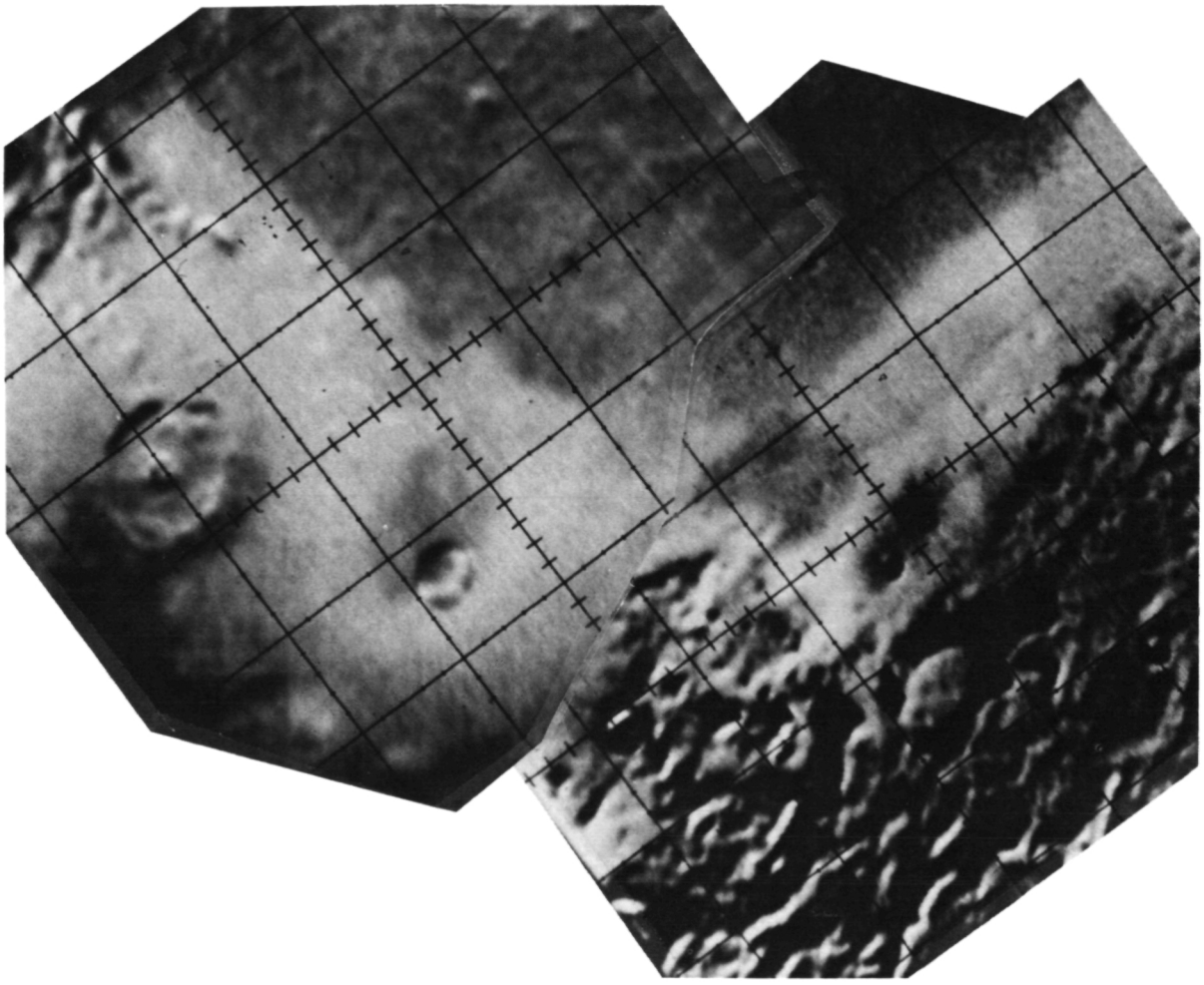

Figure 8a.—*A photographic representation of the ratio of two digital images made through an interference filter centered at 0.35 and 0.56 μm. The MITPAL silicon vidicon imaging system was used at the 88-in telescope at Mauna Kea Observatory, Hawaii. The digital images are calibrated and then divided to produce a ratio image. Here bright indicates higher untraviolet reflectances. The southeastern corner of Mare Serenitatis is shown to be about 2 km resolution. The ratio image is contrast-enhanced to show color differences of less than 1 percent.*

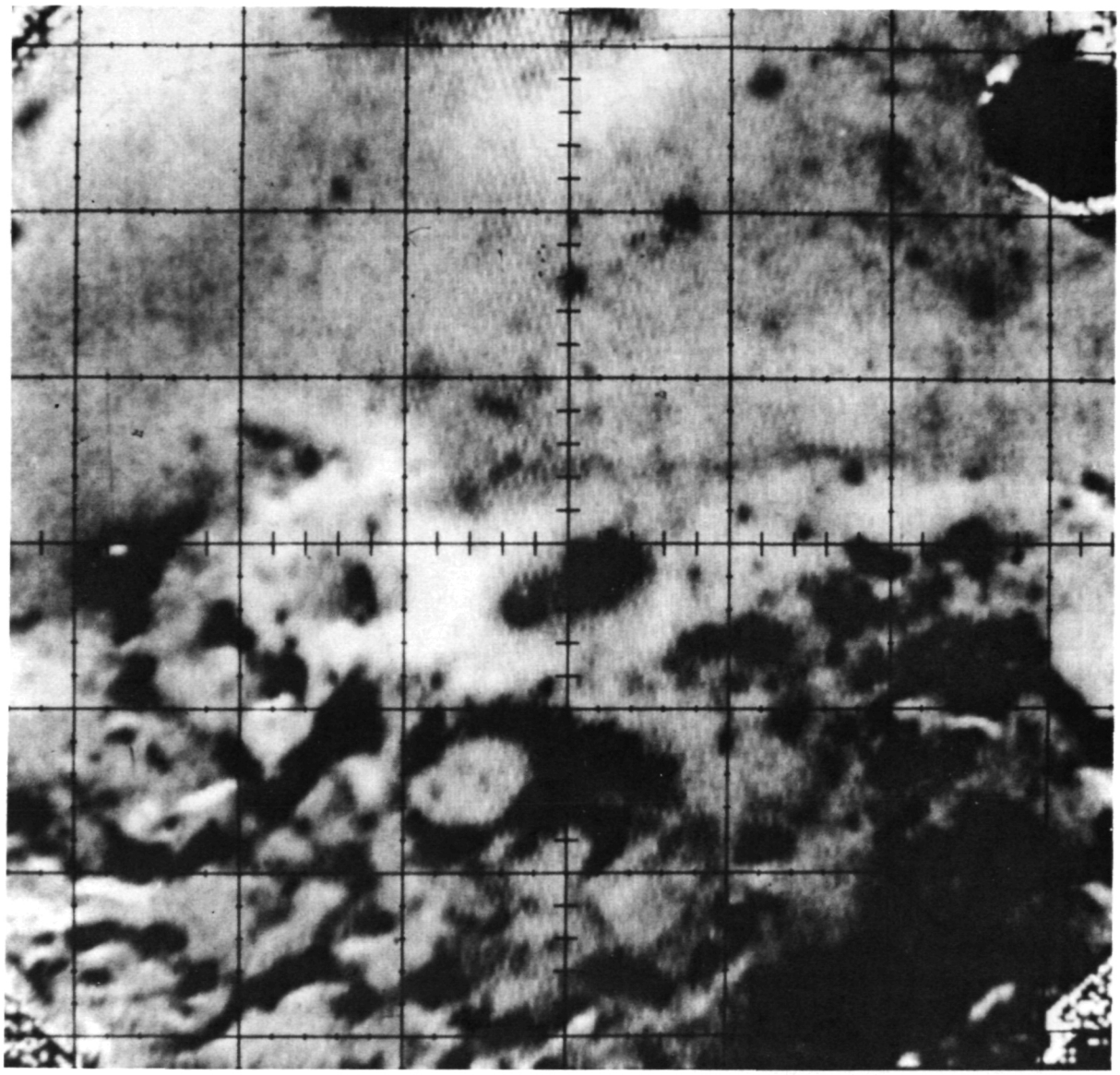

Figure 8b.—*A similar ratio image made using images at 0.95 μm and 0.56 m. Only the northern half of the image in (a) is shown. Note how the different compositional units appear in different color ratio images.*

bring out fine detail. It is of interest to note how the high titanium, dark mantling deposit near the Apollo 17 landing site stands out so prominently in this ratio image. Maps of other parameters, such as absorption band depth, can also be made. Figure 8b is the ratio image 0.95/0.56μm for a part of the same area as figure 8a. Notice that geologic units discernible in one ratio image may not be in another. Measurements of the complete spectrum for areas within these images confirm the digital color difference images to about 1 percent.

These digital color difference maps display three different compositional units in the mare near the Apollo 17 landing site in the Taurus-Littrow Valley: Central Mare Serenitatis basalt with $TiO_2 \simeq 2$ percent; Apollo

11-Mare Tranquillitatis-like basalt forming the dark ring around part of Mare Serenitatis with $TiO_2 \simeq 8$ percent; and a dark mantling unit which covers a region outside the Taurus-Littrow Valley, with $TiO_2 \simeq 12$ to 15 percent. This map has been used to show that the dark mantling unit does not extend into the Taurus-Littrow Valley at the Apollo 17 site with nearly the concentration that exists outside the valley. This explains why only remnants of the dark mantling material were found in the Apollo 17 samples (ref. 39).

Mercury

The experience gained working with telescopic and sample measurements of the Moon gives confidence to proceed to the study of other solar system objects using the same techniques. Observations of the optical albedo and polarization of the surface of Mercury have been interpreted in the past to indicate a lunar-like surface material, dark and backscattering (ref. 43). The spectral reflectance of Mercury (fig. 9) tells a similar, but more complete, story (refs. 44 and 45). The Mercury spectrum, when compared with the spectral reflectance for typical lunar mare and upland regions, indicates a lunar-like soil.

The lunar spectral reflectivity curves for mare and upland material have two major features: a uniform positive slope and a shallow absorption band near 0.95μm. A study of lunar surface material has shown that the slope of the spectral reflectivity curve for the Moon is controlled by glass containing titanium and iron in the lunar soil, and that the absorption band at 0.95μm is mainly an expression of the mineral pyroxene in the soil.

The close similarity of the features in the reflection spectra of Mercury and the Moon strongly suggests a similarity in the mineralogy and composition of their soils. Titanium- and iron-bearing glasses created by impact should be common on Mercury. This is further supported by the fact that Mercury has a low albedo similar to that for the integral nearside of the Moon. The weak 0.95-μm absorption band in the spectra of Mercury indicates that pyroxene is the major mafic mineral responsible for the band. The presence of dark glasses suggests that titanium-rich and iron-rich minerals such as ilmenite were there to be vitrified. The 0.95-μm band suggests that some crystalline pyroxenes still remain. All of this implies a heavily impacted, mafic silicate component to the surface material of Mercury. The recent Mariner 10 images of Mercury show surface features and albedos which support this conclusion reached several years before the Mariner 10 mission was flown.

Mars

A recent review of data on the Martian spectral reflectance was presented several

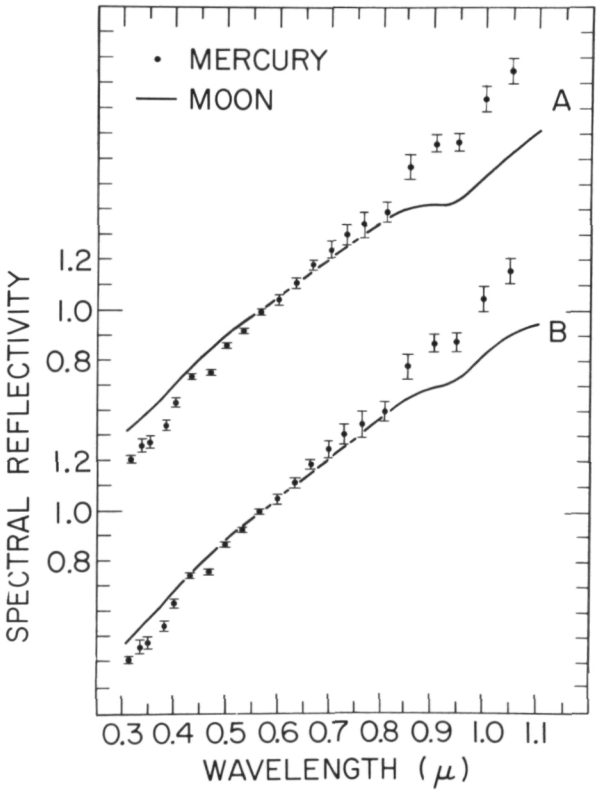

Figure 9.—*The spectral reflectivity of Mercury scaled to unity at 0.564 μm (filled circles) is compared with the reflection spectra for two different lunar terrains: (a) maria and (b) uplands.*

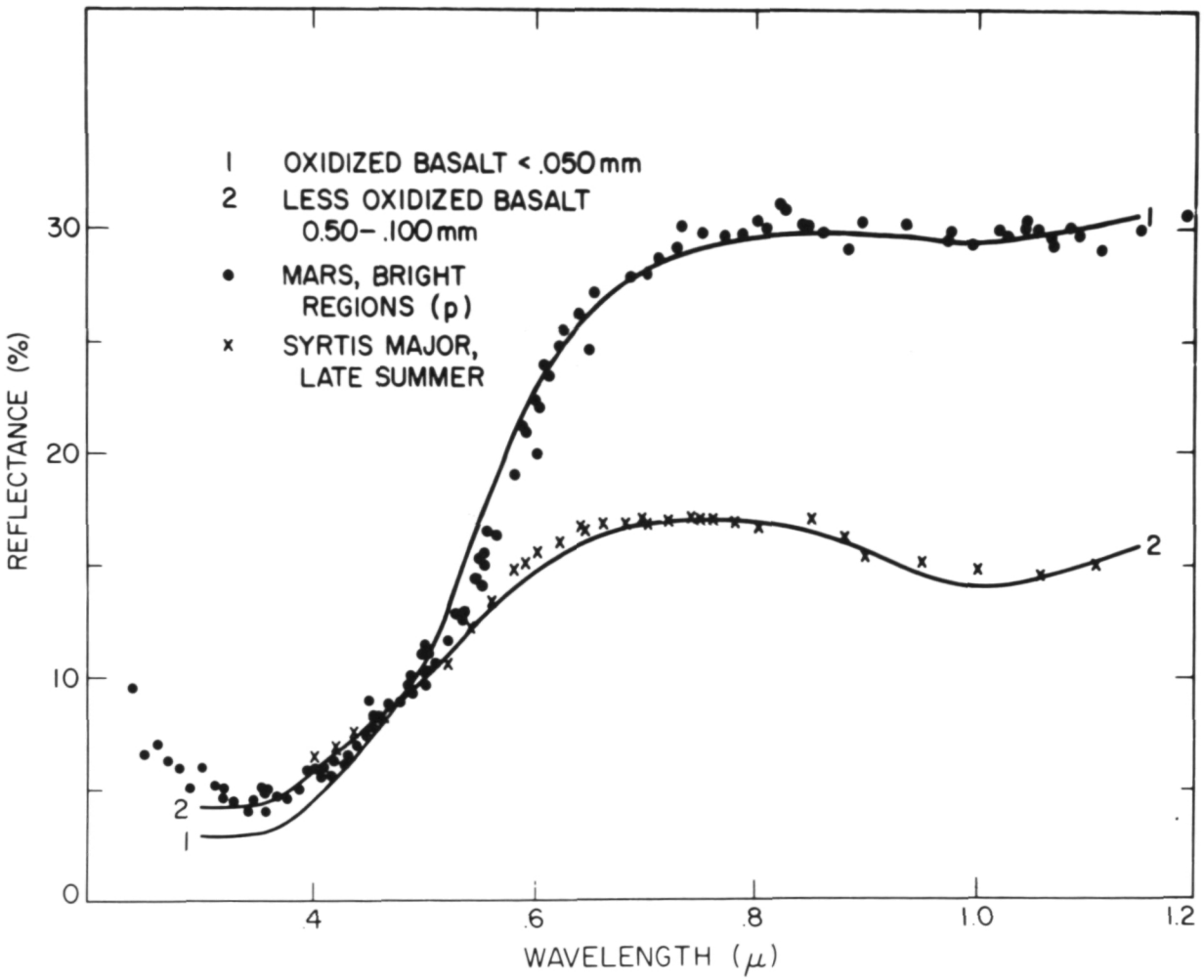

Figure 10.—*Comparison of geometric albedo curves for bright and dark areas of Mars with laboratory reflectivity curves for oxidized basalt.*

years ago (ref. 46). The spectral reflectance (0.3–1.1μ) was developed for bright material (Arabia) and dark material (Syrtis Major) (fig. 10). The curves for the bright and the dark regions of Mars show two major absorption features. Strong absorption occurs in the blue and ultraviolet. A second absorption band centered at 1μ is stronger in the dark areas than in the bright areas. These were interpreted to indicate both regions are composed of a combination of ferric iron oxide and mafic silicate rock such as basalt (ref. 47). The line superimposed on the telescope points is the reflectance spectra of the modeling materials.

We have modeled the geometric albedo curves and the normal reflectivity curves for both the bright and dark Martian areas. It is well known from laboratory studies that the ferric oxides alone cannot match the bright-area curve. Adams (ref. 18) proposed that oxidized basaltic rock could account for the blue-UV and the 1-μ absorption bands, as well as the overall curve of the bright areas. A fresh dense olivine basalt from Little Lake, California (described in ref. 17), was found to reproduce two of the essential features of the Mars curves: the 1-μ band (which in this case is contributed by olivine) and a reasonable integral reflectance when

particulate. Aside from the 1-μ band, the curve for this rock is essentially flat in the visible and near infrared.

To approximate the Martian curves, it was necessary to introduce the blue-UV Fe^{3+} band by adding ferric iron oxide and to adjust the integral reflectance by changing particle size. With the results of the laboratory study it was possible to achieve a close fit to the Martian curves for both the bright and dark areas (fig. 10). We were not able to approximate the Martian curves in the laboratory with any materials other than the oxidized basalt. In fact, of the eight basalts tried, only the olivine-bearing Little Lake basalt was satisfactory. Our experiments have shown that the Mars curves cannot be produced simply by various nonunique combinations of materials. If one is constrained to reproduce in the laboratory the several absorption bands and between-band structures that appear in the new Mars curves (rather than considering any single band), and, furthermore, if the modeling materials must be geochemically reasonable, then the possible solutions are severely limited.

We concluded that both the dark and the bright areas of Mars can be modeled by the same fundamental material (here the basalt), provided that the material modeling the bright regions is the more oxidized and has a smaller mean particle size ($< 50\mu$).

Spectral reflectance curves for seven Martian regions were obtained during the 1969 opposition (ref. 48). Geometric albedos were calculated for five areas between 0.3 and 1.1μ and for two additional areas between 0.3 and 2.5μ. These were compared with earlier measurements and were found consistent (ref. 49). During the 1973 opposition, approximately 25 additional Martian areas were measured between 0.3 and 1.1μm (ref. 50). Again the results are consistent with earlier data.

The spectra of three of the bright areas are presented in figure 11a. All display a strong blue-UV absorption feature, with a band center near 0.45μm, a band edge near 0.8μm, and slope changes at about 0.5μm and 0.6μm. The spectra display a weak absorption band near 0.95μm, with the reflectance at 1.1μm approximately equal to the reflectance at 0.8μm and equal to about twice the reflectance at 0.57μm. Three of the dark-area spectra are shown in figure 11b. Each of the dark-area spectra displays a blue-UV absorption feature centered near 0.45μm. The blue-UV band edge in the dark-area curves occurs near 0.7μm. There is a broad absorption envelope in the 0.9- to 1.1-μm region, with the reflectance at 1.1μm about 10 to 20 percent lower than the reflectance at 0.7μm and only about 1.3 to 1.4 times the reflectance at 0.57μm.

Mariner 9 IRIS spectra of the high albedo dust which was raised from the surface into a planetwide dust storm in 1971 (ref. 51) indicates an SiO_2 content of 60 ± 10 wt% (ref. 52) concluded from the shape and position of the 9-μ Reststrahlen band that the principal constituent was montmorillonite. Both of these interpretations are consistent with one another and with the infrared spectroscopic evidence for widespread hydrate minerals on the surface (ref. 53).

The soils in the bright areas of Mars appear to be highly weathered according to both the Earth-based and spacecraft data. The reflectance spectra of 200-km-diameter spots in the dark areas indicate that the soils in these regions are not as weathered. The presence of clay minerals (kaolinite, montmorillonite) are consistent with our early analysis and a more recent analysis (ref. 54) of the new reflectance data, although more work is needed before a detailed interpretation can be given. It is clear that hydrated iron oxide is present.

One model which has been generally suggested to account for the presence of ferric oxides and widespread hydrate minerals is that these materials are metastably preserved from an early epoch when Mars had a wetter, more oxidizing Earth-like environment. An alternative model has been proposed by Huguenin (ref. 55), who suggests that the present-day Martian surface environment has a sufficiently high oxidation potential.

Based on a series of laboratory experi-

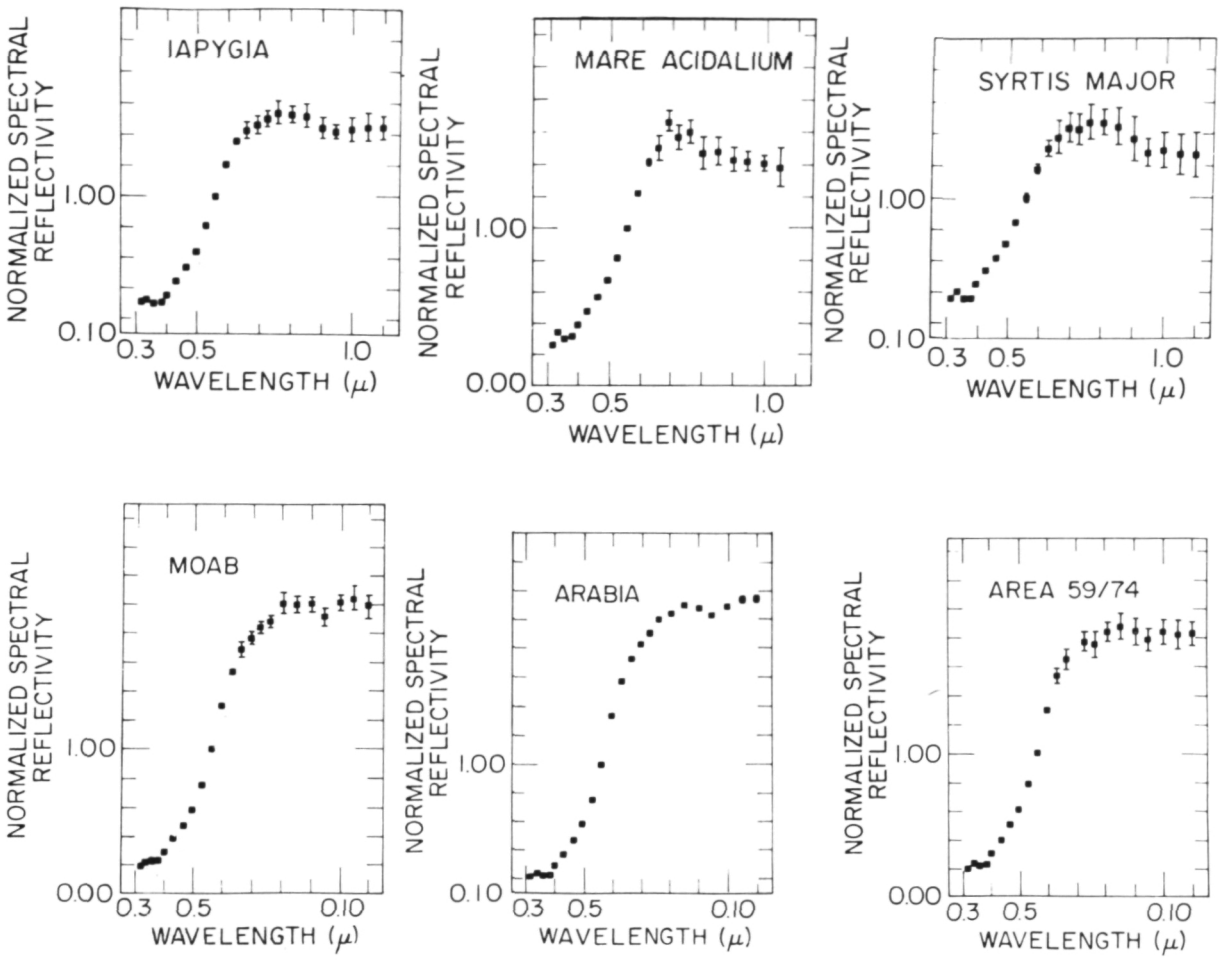

Figure 11.—*Spectral reflectance for three bright regions (lower plots) and three dark regions (upper plots) about 200 km in diameter on the surface of Mars. See reference 49 for location.*

ments, Huguenin (refs. 55, 56, and 57) predicts that reduced-state metal oxides (magnetite, ilmenite) and ferrosilicates alter to hydroxylated and hydrated oxides and clay minerals upon exposure to absorbed H_2O, solar UV-illumination, atmospheric O_2, and eolian abrasion, through a process called "photostimulated oxidation weathering."

In an attempt to map the spectra features found to indicate composition on the Martian surface, the same vidicon digital imaging system used on the Moon was used to observe Mars during the fall of 1973. Although many images were obtained through interference filters centered at 25 wavelengths between 0.34 and 1.1μm, only a few have been analyzed at this writing. The series of images shown in figure 12 indicates the quality of images possible with 1-percent photometer precision. The clouds and dust storms visible reveal an unexpected bonus from this type of two-dimensional photometry. These images are presently being used to determine characteristics of dust clouds and related surface material.

The Asteroids

It has long been realized that studies of the colors of asteroids provide useful clues to their composition (refs. 58 through 62). Until recently, attempts to determine asteroid composition by comparing color indices

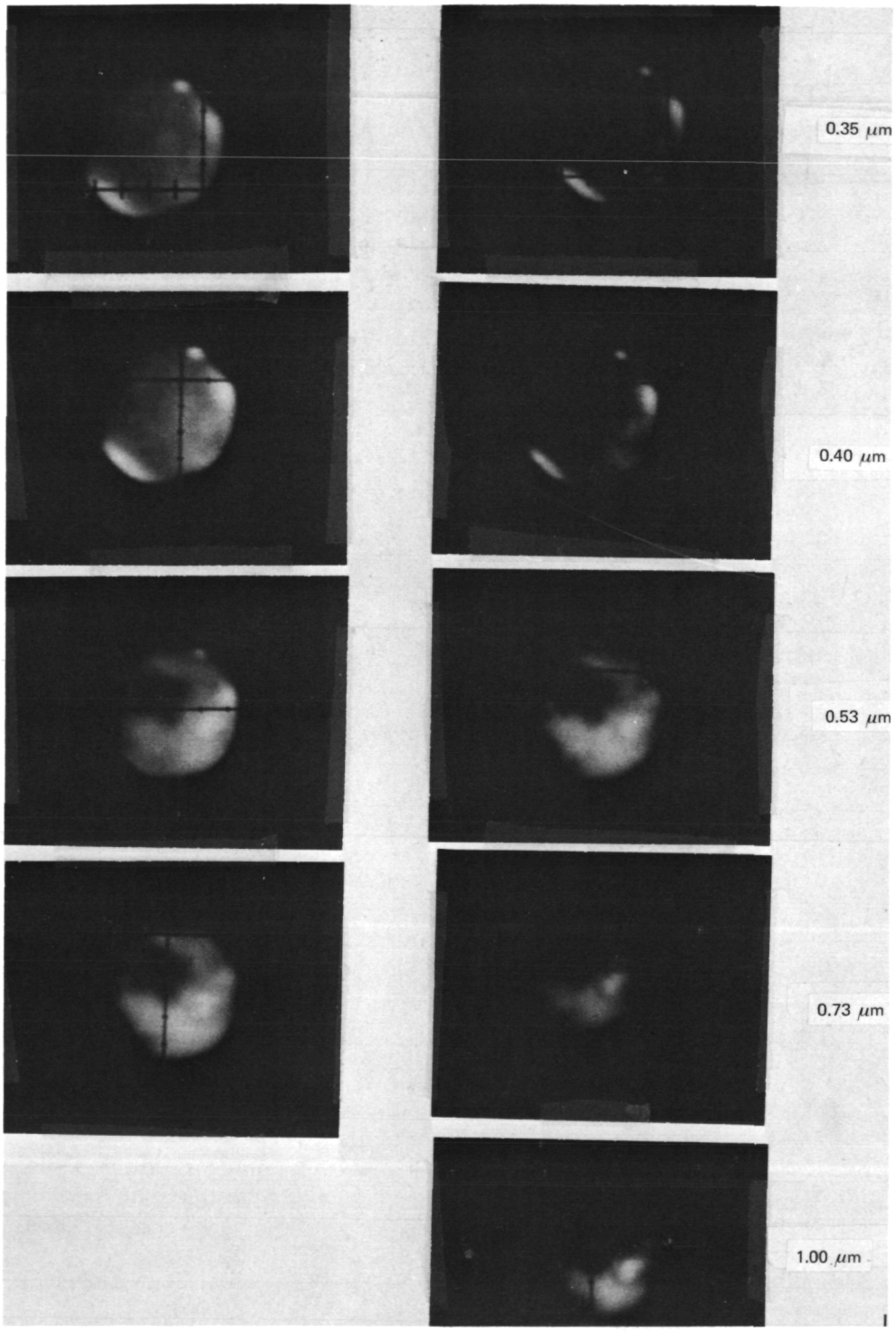

Figure 12.—*Photographic representations of a series of digital images of Mars using the MITPAL silicon vidicon imaging system. Images were made throughinterference filters centered at 0.35, 0.40, 0.53, 0.73, and 1.00 μm using the 88-in telescope at Mauna Kea Observatory, Hawaii, during the 1973 opposition. Surface features and clouds are visible.*

for asteroids with spectral reflectivities or color indices for meteorites and terrestrial rocks have not been fruitful (ref. 10). It has been noted that the mean color indices for asteroids fall within the range for rocks and meteorites. However, there are far too many minerals for a one-dimensional characterization of asteroid color (color index) to suggest even a compositional class, let alone a specific composition.

McCord, Adams, and Johnson (ref. 1) reported on the observation and analysis of the spectral reflectance of the asteroid Vesta between 0.32 and 1.1μm, with spectral resolution and photometer precision sufficient to show a number of important absorption features. A strong absorption band is centered near 0.9μ, and a weaker absorption feature appears between 0.5 and 0.6μ. The reflectance decreases strongly in the ultraviolet. The strong 0.9-μ band arises from electronic absorptions in ferrous iron on the M2 site of a magnesian pyroxene. Comparison with laboratory measurements on meteorites and Apollo samples indicates that the surface of Vesta has a composition very similar to that of certain basaltic achondrite meteorites (fig. 13).

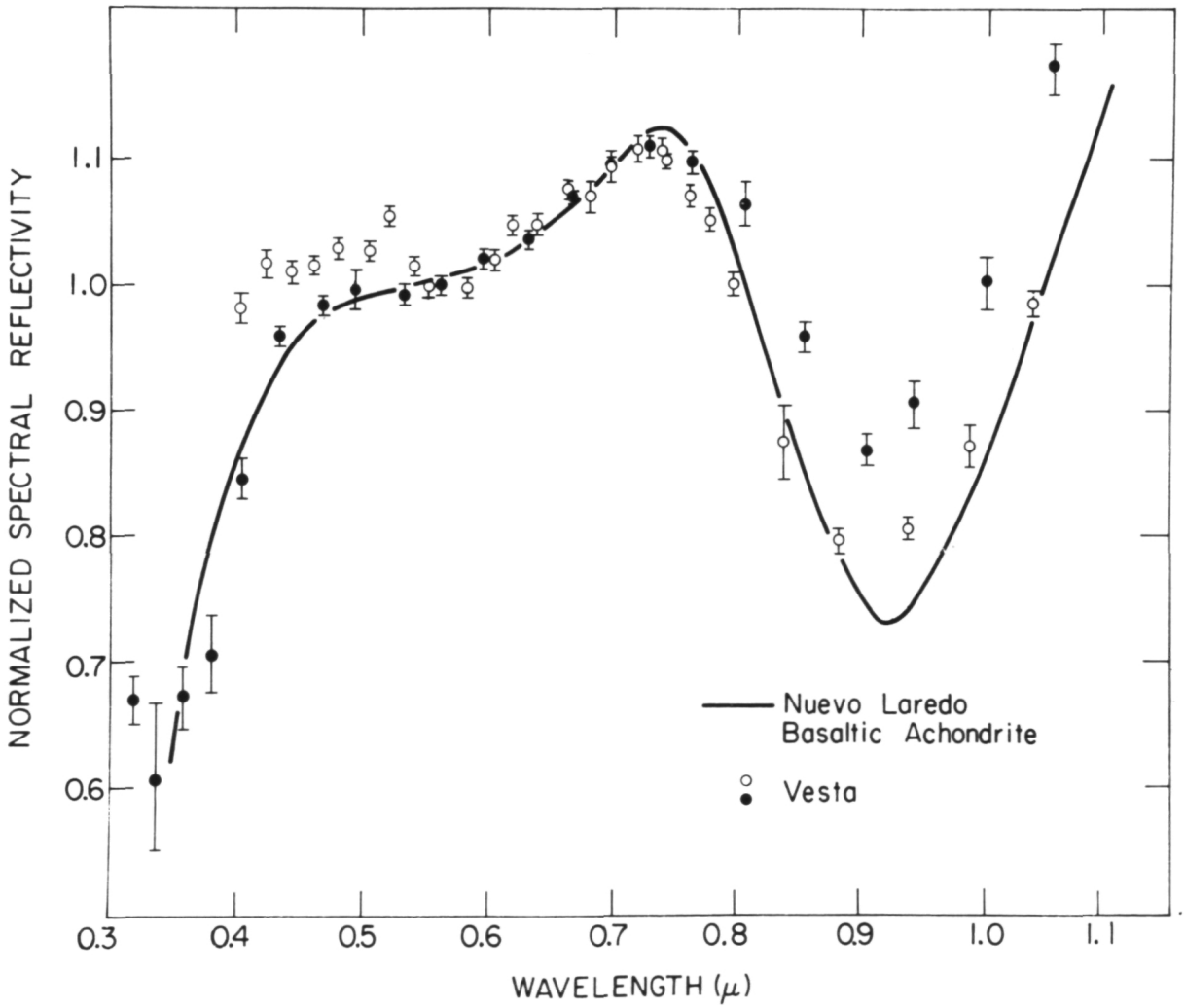

Figure 13.—*Laboratory measurements of the spectral reflectivity of the Nuevo Laredo meteorite shown with the telescope data.*

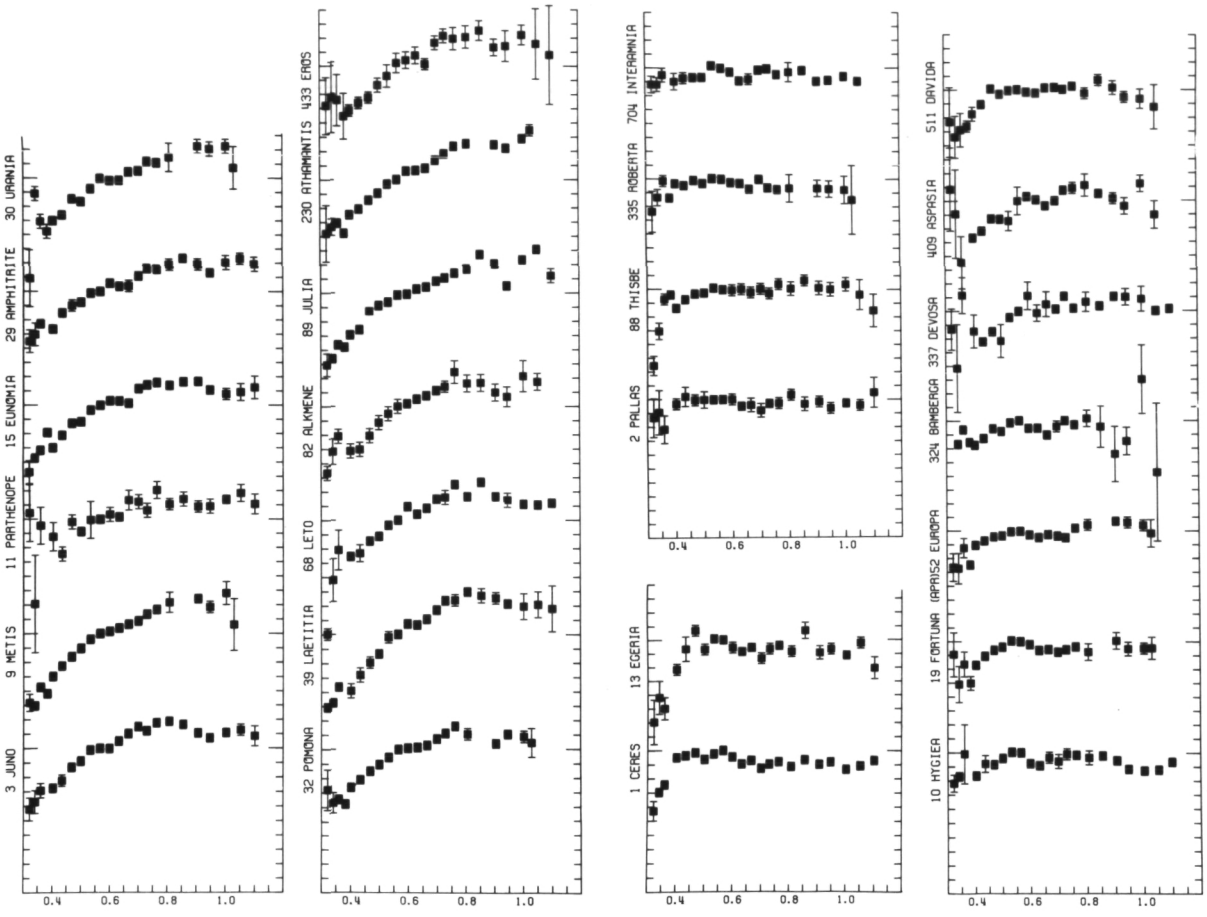

Figure 14a,b.—*Spectral reflectance of several asteriods showing a variety of curve shapes.*

An extensive program has been underway in our laboratories since this discovery to obtain reflection spectra for many asteroids using ground-based telescopes. So far, about 100 asteroids have been observed (refs. 10, 63, and 64). Various spectral reflectance curves for asteroids are shown in figure 14.

The early work with Vesta has suggested the direct relation between meteorites and asteroids. The mineral assemblages found in meteorites should, on cosmochemical arguments, represent a mineralogical and petrological series which shares many of the compositional characteristics of asteroidal material. Therefore, to expand the laboratory and theoretical basis for interpreting the reflectance spectra for asteroids, a study was made of the optical properties of 156 meteorite specimens from essentially all meteorite classes (refs. 26 and 27). The meteorite spectra are grouped in figure 15 according to class and therefore according to mineralogy. Note that the variation of the spectra within a class is less than the differences between classes. Metamorphic grading and changes in mineralogy through the classes are easily seen in the spectra.

The reflectance characteristics of meteorite curves are understandable in terms of the type, composition, abundance, and distribution of the component mineral phases. Four classes of minerals can be defined on the basis of their contribution to spectra of mixtures of phases: metals, opaques, and silicates with and without transition metal ions such as Fe^{2+}. The effect a mineral has on the

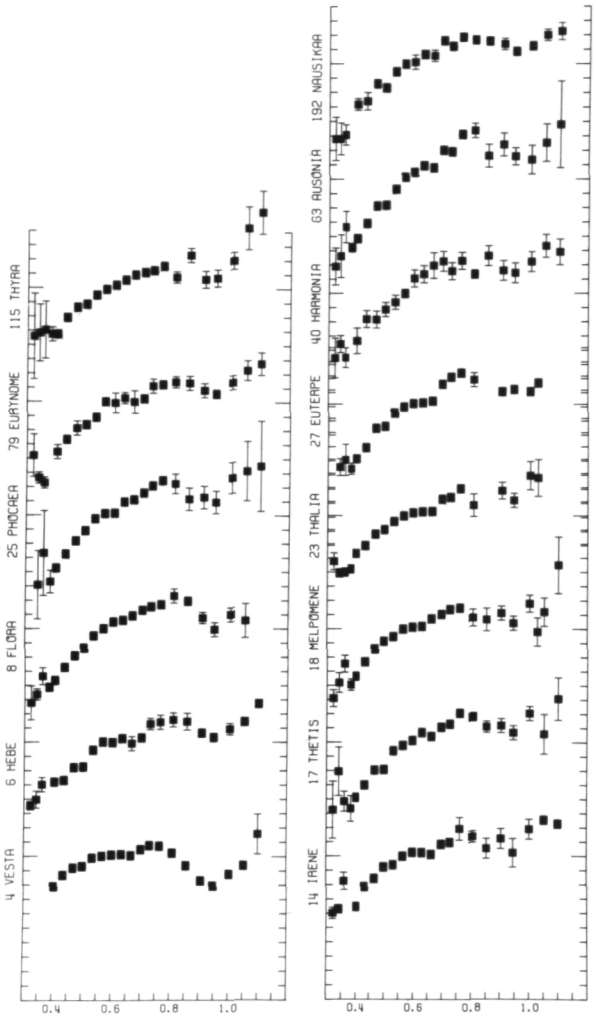

Figure 14c.—*Spectral reflectance of several asteroids showing a variety of curve shapes.*

spectrum is approximately proportional to its abundance and its optical density in the spectral region of interest. Opaques, most commonly represented by carbon and the carbon compounds, tend to dominate a spectrum even when present in small quantities (a few percent). Opaques produce low reflectances throughout the visible and infrared spectrum and have a relatively strong ultraviolet absorption. Silicates containing transition metal ions (pyroxene, olivine, feldspar) exhibit crystal field absorption features near 1μ. The wavelength position of the bands depends on the composition of the mineral. These silicates are also characterized by increasingly more efficient charge transfer absorptions as one moves toward higher energies. Metals (Fe, Ni) become steadily more reflective toward longer wavelengths and exhibit a very nearly linear change in reflectance with energy.

Previous spectral reflectance work on meteoritic materials, primarily by Hunt and Salisbury (ref. 65), Chapman and Salisbury (ref. 66), and Johnson and Fanale (ref. 67), provides good agreement with this work in the areas where there is overlap.

The philosophy applied in our study (ref. 68) is to interpret absorption features in the asteroid curves in terms of the minerals producing or modifying each feature. A set of features reveals a suite of minerals, which defines a rock type in many cases. This rock type may or may not conform to the definition of an established meteorite class. This approach does not rely on the match of asteroid spectra with meteorite spectra. The meteorite sample material, which is used to study the optical properties of solids, is used as a source of mineral assemblages which are cosmochemically reasonable to occur in the asteroid belt. Blind curve matching without understanding the physical explanation for each spectral feature often leads to error.

The interpretation of two asteroid reflection spectra is treated here (fig. 16). The same procedure has been applied to other spectra (ref. 68).

1 Ceres: The uniform visible and infrared reflectance and the strong ultraviolet absorption indicates, and for meteoritic material is characteristic only of, the higher grade carbonaceous chondrites (right column, bottom). Ceres' surface is composed of a mineral assemblage rich in opaque material (probably carbon) and probably is a type of carbonaceous chondrite material.

3 Juno: This spectrum is characterized by a more or less linear increase in reflectance with wavelength, a relatively strong, broad, asymmetric absorption near 1.0μm, and a weak absorption near 0.6μm. The linear reddening indicates a large metal component, and the absorption features near 0.60, 0.95,

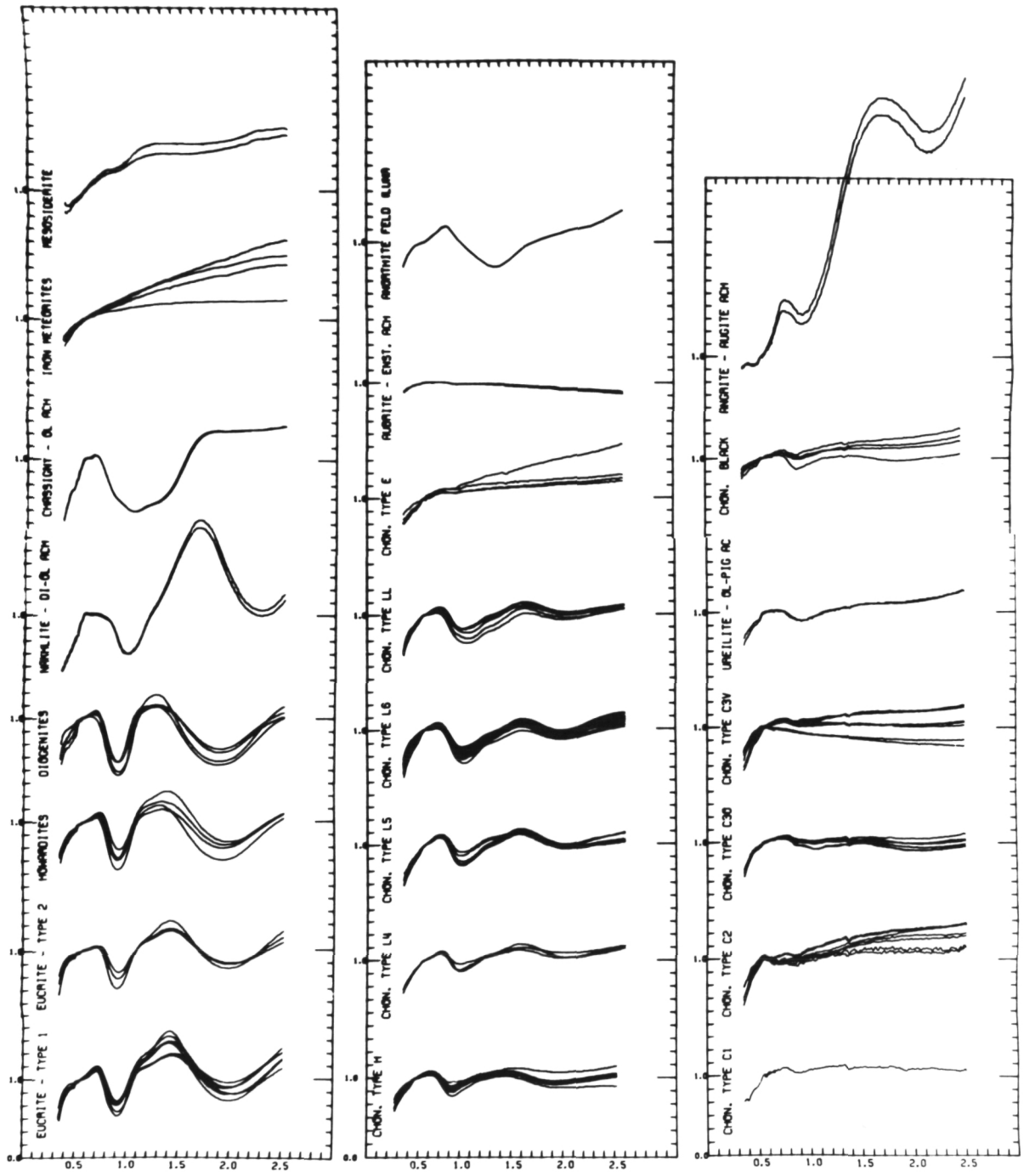

Figure 15.—*Spectral reflectance of 156 meteorite specimens grouped according to mineralogy and meteorite class. All samples were carefully studied to eliminate weathered or otherwise damaged samples.*

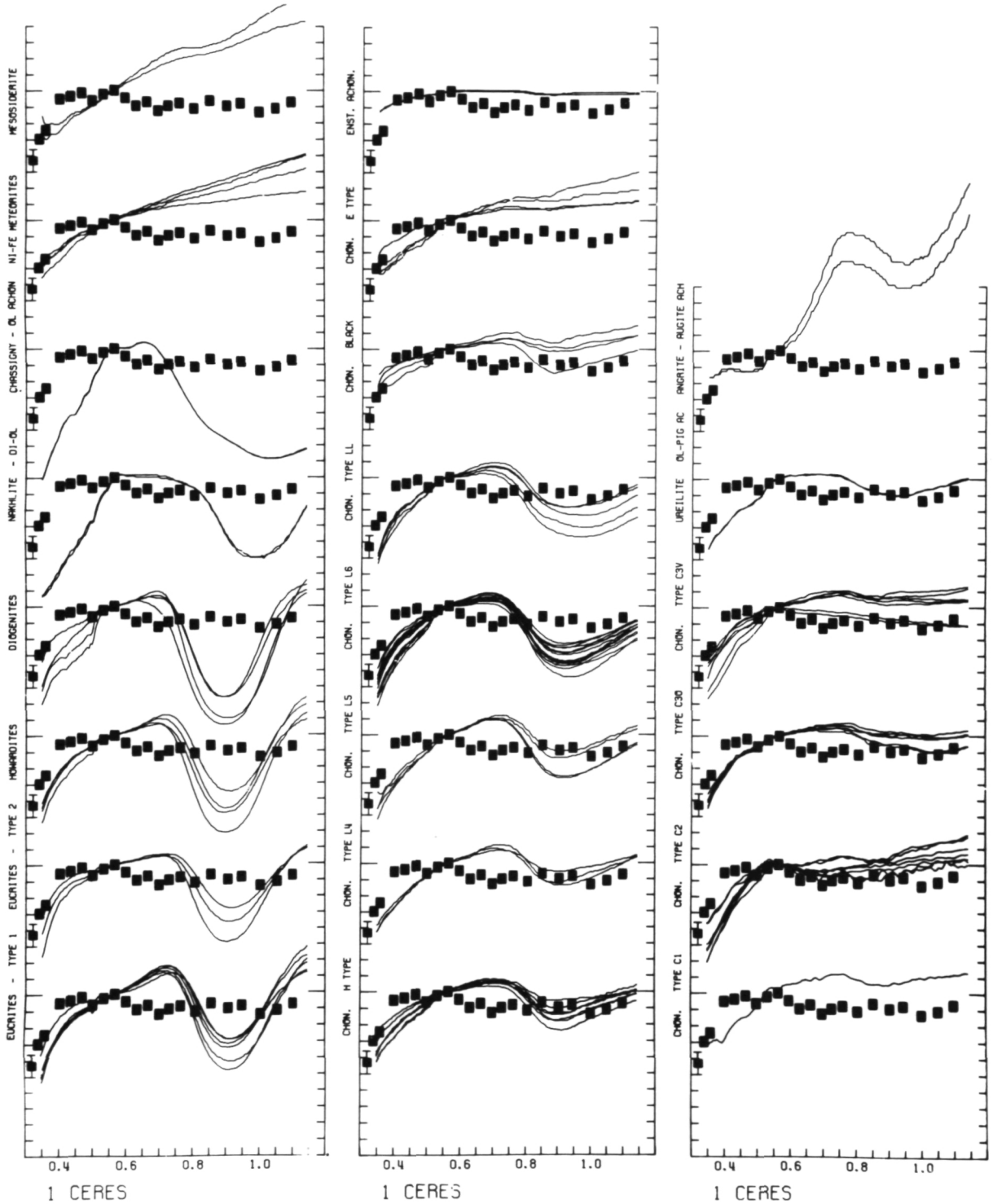

Figure 16a.—*Spectral reflectance for asteroid 1 Ceres, superimposed on the spectra for 156 meteorites. The meteorite spectra are arranged according to class. Reflectance is plotted against wavelength in micrometers. Each division in reflectance is 0.1. All curves are scaled to unity at 0.56 μm.*

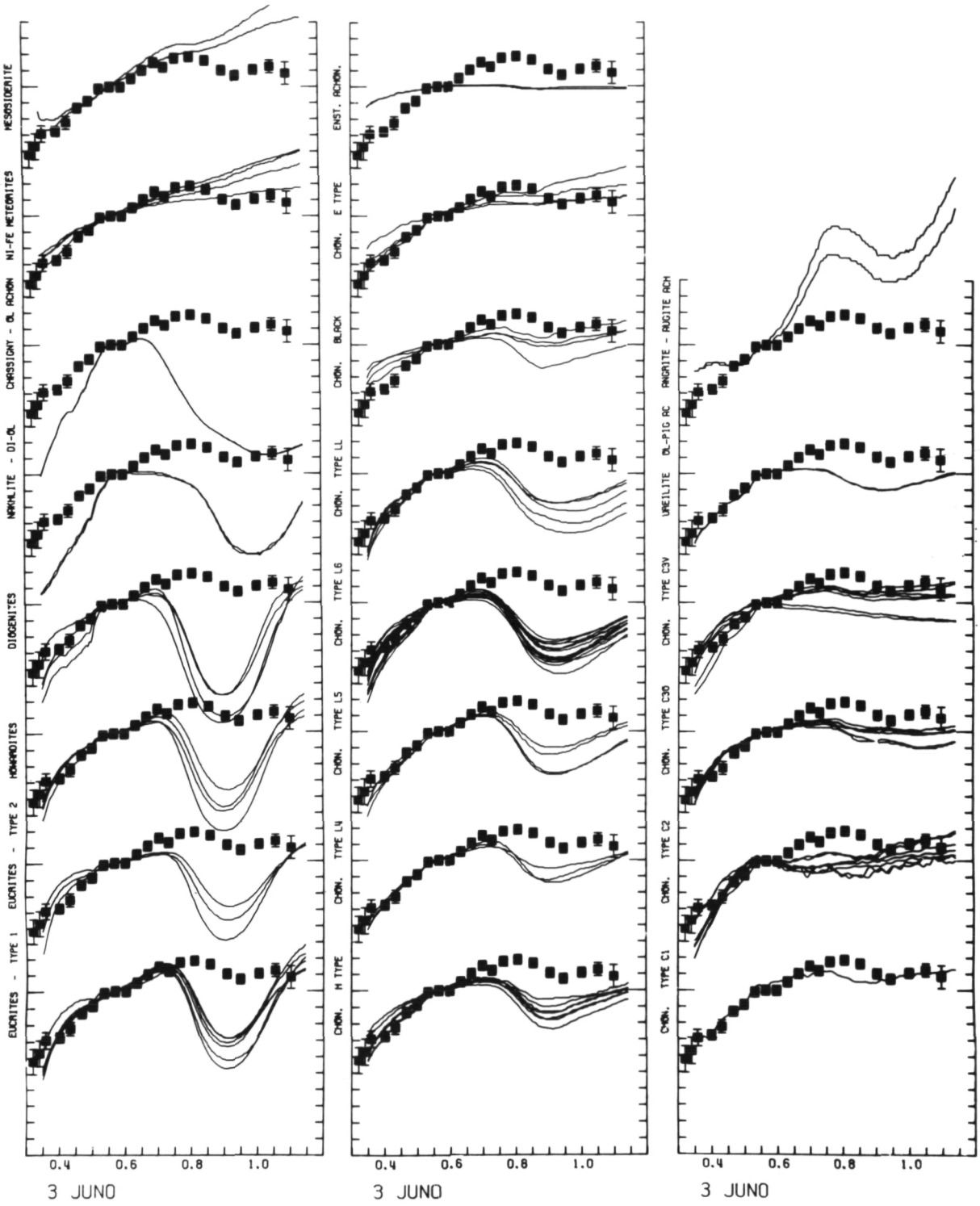

Figure 16b.—*Spectral reflectance for 3 Juno superimposed on the spectra for 156 meteorites. The meteorite spectra are arranged according to class. Reflectance is plotted against wavelength in micrometers. Each division in reflectance is 0.1. All curves are sealed to unity at 0.56 μm.*

and 1.1μm indicates plagioclase, pyroxene, and olivine, respectively. The modification of the spectrum of an iron meteorite by the addition of the silicate absorption would produce the best agreement with meteorite material. This is an example where the direct matching technique is inappropriate and would produce spurious results.

The preliminary analysis that has been made indicates several conclusions about the asteroids. The mineral assemblages that appear to compose the asteroids are similar to those found in meteorites. However, it is clear that the population of meteorite classes is not the same as for asteroids. For example, in the asteroid belt there appear to be many objects with composition similar to carbonaceous chondrites, but very few objects similar to ordinary chondrite meteorites, unlike the distribution of compositions of meteorites. The one asteroid measured with a chondritic surface is Toro (ref. 63), an Apollo asteroid. This may be a hint of the origin of most meteorites.

It also appears that asteroids are mostly homogeneous over their surfaces; i.e., all sides seem to have similar composition. There is little difference in the spectral reflectance with rotational phase for the vast majority of asteroids measured. However, there are striking differences among asteroids. Inner-belt asteroids appear to be more commonly of high-grade iron-silicate composition, while outer-belt asteroids are more often of more primitive carbonaceous chondrite nature.

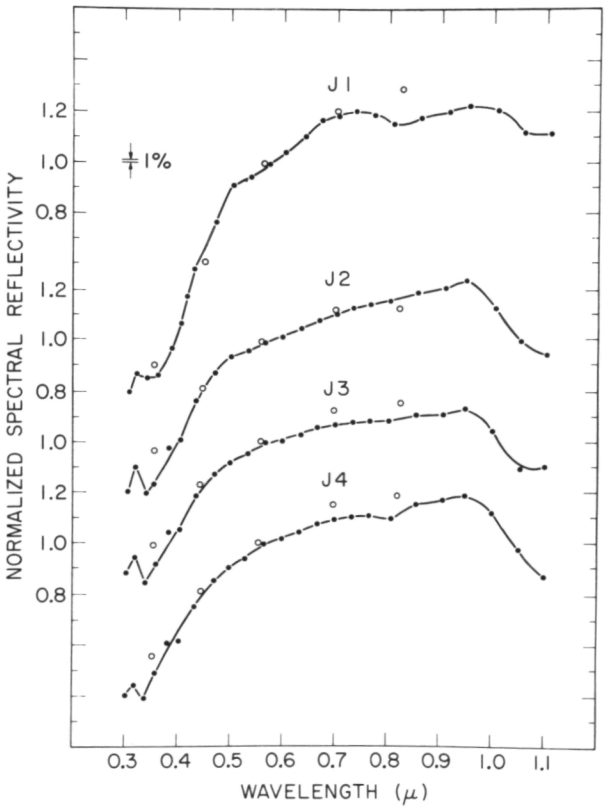

Figure 17.—*Normalized spectral reflectivity 0.3 to 1.1 μm for the Galilean satellites.*

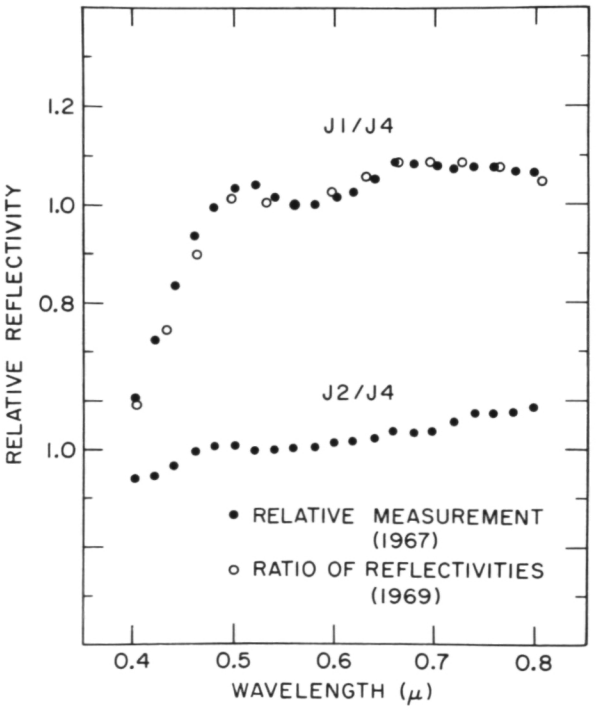

Figure 18.—*Normalized relative reflectivities for J1 versus J4 and J2 versus J4. Filled circles are direct double-beam measurements, and the open circles are ratios of individual reflectivity curves.*

Jupiter Satellites

In the outer solar system we see a different kind of material than is present in the inner solar system. For example, in figure 17 is shown the spectral reflectance for the Galilean satellites, the four largest satellites of Jupiter. They are the only ones bright enough to be easily studied. The spectral reflectance for the 0.3 to 1.1μm spectral region (refs. 69 and 70) is unlike any spectrum seen so far in this discussion (fig. 17). The strong UV absorption is reminiscent of the charge transfer feature found for iron silicates, but the match is really quite poor. The shallow absorption band seen (especially for Io) (fig. 18) between 0.5 and 0.6μm was also a puzzle.

The reflection spectrum was measured more recently from 1.0 to 2.5μm (refs. 71 and 72) (fig. 19). Water frost absorptions were detected in the infrared reflectivities of Jupiter's Galilean satellites JII (Europa) and JIII (Ganymede). The percentage of frost-covered surface area was determined to be 50 to 100 percent for JII, 20 to 65 percent

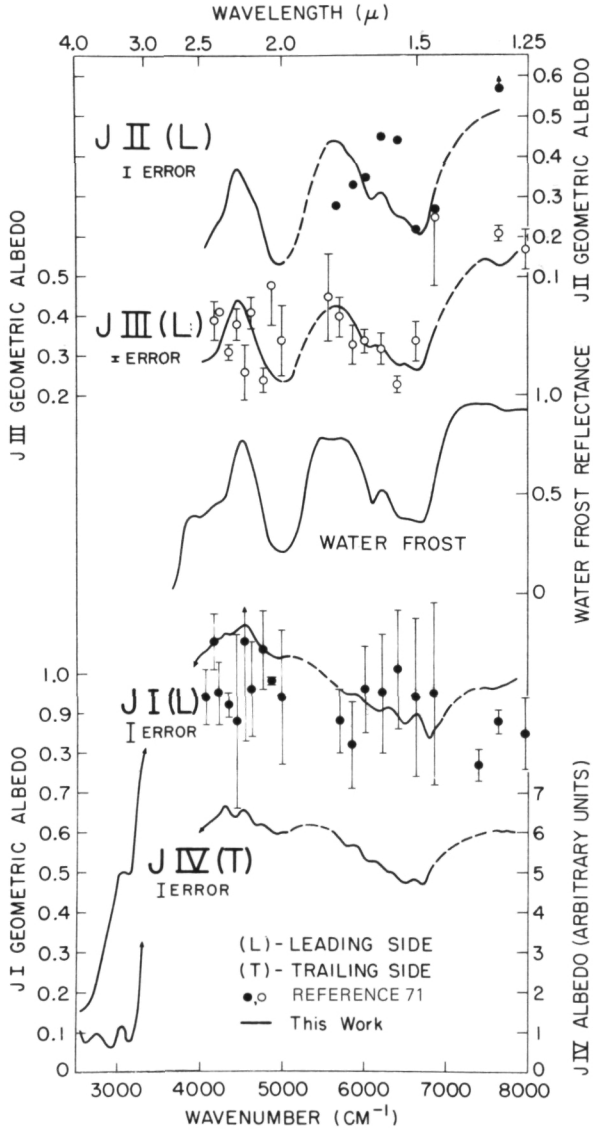

Figure 19a.—*Reflectivities of the Galilean satellites and water frost. The reflectivities of JI, JII, and JIII have been scaled approximately to the geometric albedos of Johnson and McCord (ref. 71). Each error bar is the average of the standard deviations for all wavelengths. The intensities of the reflectivities of JI and JIV between 2500 and 3300 cm^{-1} are reduced to an MgO standard.*

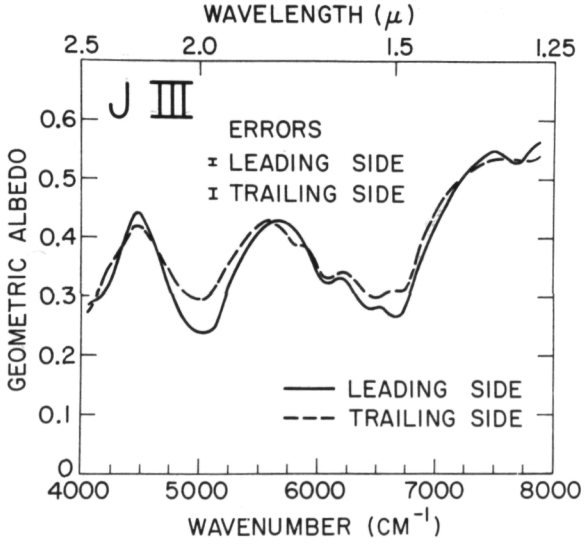

Figure 19b.—*The reflectivities of the leading and trailing sides of JIII scaled to the same value at 5625 cm^{-1}. Both reflectivities are also scaled to the geometric albedos of Johnson and McCord (ref. 71). Each error bar is the average of the standard deviations for all wavelengths.*

for JIII, and possibly 5 to 25 percent for JIV (Callisto). The leading side of JIII has 20 percent more frost cover than the trailing side, which explains the visible geometric albedo differences between the two sides. The reflectivity of the material underlying the frost on JII, JIII, and JIV resembles that of silicates. The surface of JI (Io) may be covered by frost particles much smaller than those on JII and JIII.

But the visible spectrum does not look anything like it should for water ice. Lebofsky (ref. 73), following suggestions from work by Lewis (refs. 74 and 75) and considerably expanding on some early work by Sills at the University of Arizona, studied the optical properties of sulfur-contaminated ices. Lebofsky irradiated these compounds with solar-like ultraviolet flux and observed color properties similar to the satellites.

Saturn Rings

The rings show a reflection spectrum quite similar to those for the Galilean satellites of

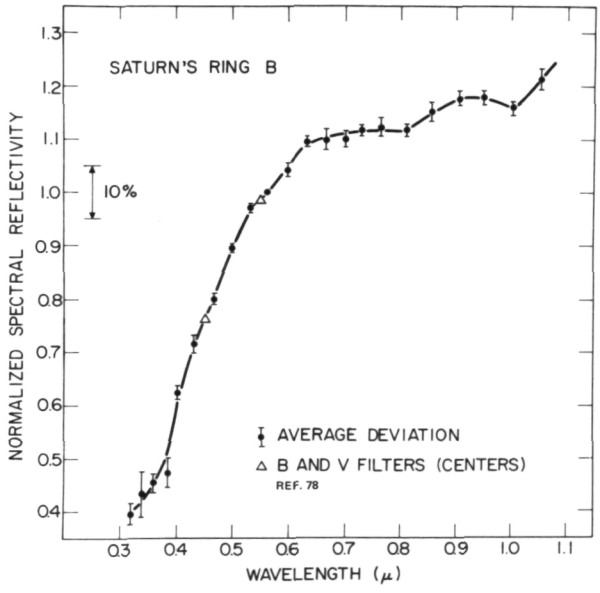

Figure 21.—*Comparison of reflectance spectra for H_2O and NH_3 frosts and Saturn's rings. The major region of disagreement between the ring and NH_3 frost spectra is indicated by a vertical line at 2.22 μ (4500 cm^{-1}). With the exception of curve III, the vertical axis is not calibrated, and sloping trends can be ignored for purposes of comparison. The vertical calibration for curve III is along the left side of the figure. Curve Ia—the Saturn ring spectrum. Curve Ib—lunar comparsion spectrum. Curve II—fine-grained H_2O frost spectrum. $\Delta\lambda \approx 0.05$ μ, $\lambda < 1.58$ μ; $\Delta\lambda \approx 0.03$ μ, $\lambda > 1.58$ μ. Curve III—normalized Saturn ring spectrum (Ia divided by Ib): the dashed portions of the curve indicate regions affected telluric apsorption. There is a gap in the curve near the saturated 2.7-μ telluric band. Curve IV—NH_3 frost spectra: (IVa) fine-grained frost; (IVb) coarse-grained frost; same resolution as in curve II.*

Figure 20.—*The normalized reflectivity of Saturn's ring B as a function of wavelength is shown. Each point represents an average of measurements through one interference filter. The standard deviation of the average value is shown as an error bar. A smooth curve has been drawn through the data points (see ref. 78).*

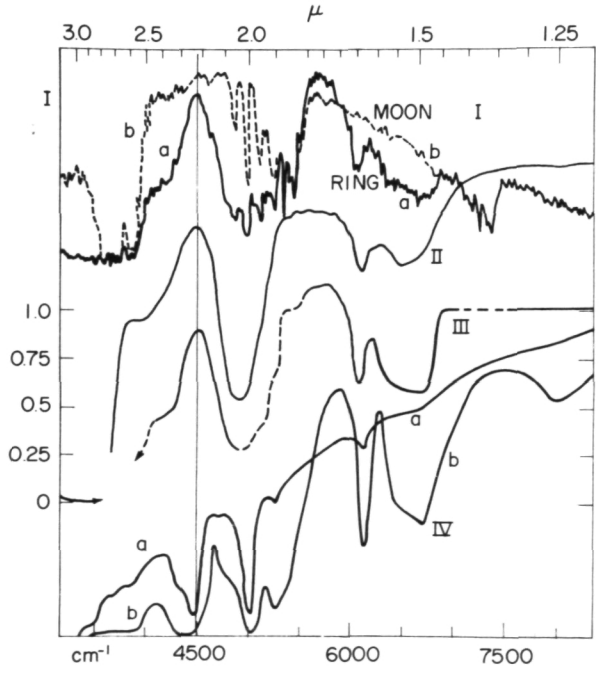

Jupiter. Between 0.3 and 1.1μm (refs. 76 and 77) (fig. 20) there appears the strong UV absorption. The infrared reflection spectrum (ref. 79) contains strong water-ice bands (ref. 80) (fig. 21). Probably the same interpretation applies as for the Galilean satellites.

Saturn Satellites

The spectral reflectance for the satellites observed is flat and featureless (ref. 76) (fig. 22). Two possibilities exist based on our past experience. The spectra are consistent with uncontaminated solid water or ammonia and these are cosmochemically quite reasonable materials. The data for the spectral region available are also consistent with carbonaceous chondritic material, another reasonable material. Spectra for the ultraviolet spectral region should determine this uncertainty (see the section on asteroids). If the conclusion is ice for the composition of the surfaces of these objects, why are the ring particles contaminated and radiation damaged and the satellites not? Perhaps because of a Saturian magnetic field.

General Comments

The data are not complete enough to discuss the remaining solar system objects that have visible solid surfaces (outer planet satellites and Pluto). Clearly these objects deserve more study considering what has been thus far possible. But measurements are difficult because of their faintness and, often, their close proximity to bright planets.

The composition of solar system objects is one of the more fundamental properties to aid in unraveling the origin and evolution of the solar system. It is our hope that this exciting task will be easier with the development of this new remote sensing technique.

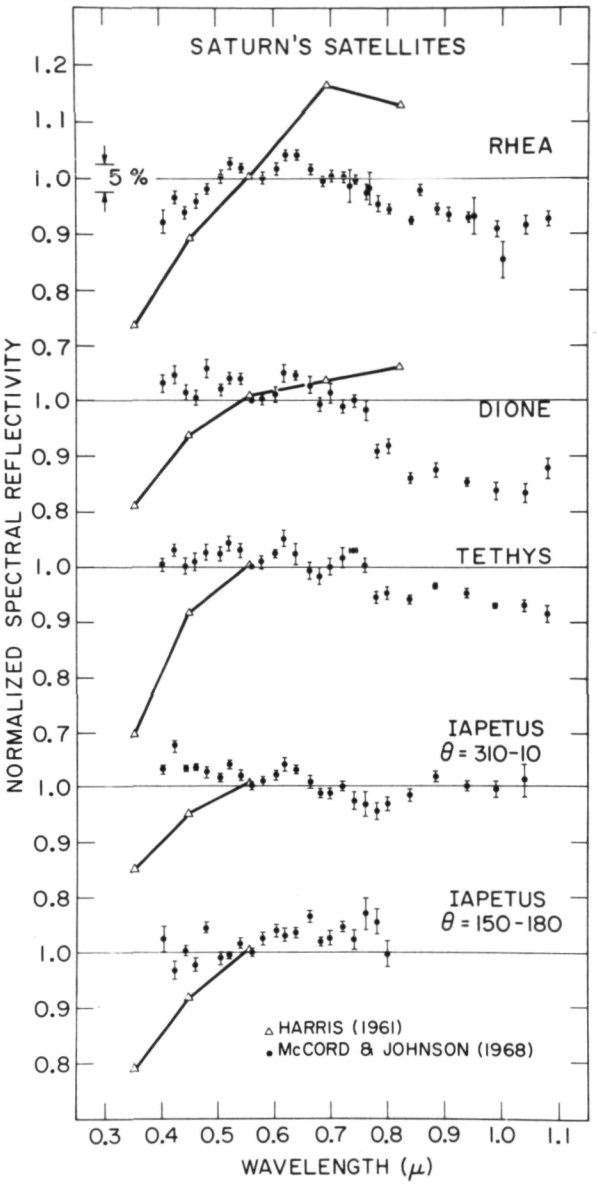

Figure 22.—*Spectral reflectance of Saturn's satellites scaled to unity at 0.56 μm.*

References

1. McCord, T. B., J. B. Adams, and T. V. Johnson, Asteriod Vesta: Spectral Reflectivity and Compositional Implications. *Science*, Vol. 168, 1970, p. 1445.
2. McCord, T. B., *Color Differences of the Lunar Surface*. Ph.D. dissertation, Calif. Inst. of Technol., Pasadena, Calif., 1968.
3. McCord, T. B., and J. A. Westphal, A Two-Dimensional Silicon Vidicon Astronomical Photometer. *Applied Optics*, Vol. 11, 1972, p. 522.
4. McCord, T. B., and J. Bosel, Silicon Vidicon Astronomy at MIT. *Astronomical Observa-*

tions With Television Type Sensors, J. W. Glaspey, and G. A. H. Walker, eds., Institute of Astronomy, Univ. of B.C., Vancouver, 1973, pp. 137–161.

5. OKE, J. B., Photoelectric Spectrophotometry of Stars Suitable for Standards. *Astrophys. J.*, Vol. 140, 1964, p. 689.
6. SCHILD, R., D. M. PETERSON, AND J. B. OKE, Effective Temperatures of B- and A-Type Stars. *Astrophys. J.*, Vol. 166, 1971, p. 95.
7. OKE, J. B., AND R. E. SCHILD, The Absolute Spectral Energy Distribution of Alpha Lyrae. *Astrophys. J.*, Vol. 161, 1970, p. 1015.
8. HAYES, D. S., An Absolute Spectrophotometric Calibration of the Energy Distribution of Twelve Standard Stars. *Astrophys. J.*, Vol. 159, 1970, p. 165.
9. ARVESEN, J. C., R. N. GRIFFIN, AND B. D. PEARSON, JR., Determination of Extraterrestrial Solar Spectral Irradiance From a Research Aircraft. *Applied Optics*, Vol. 8, 1969, p. 2215.
10. CHAPMAN, C. R., T. B. MCCORD, AND T. V. JOHNSON, Asteroidal Spectral Reflectivities. *Astron. J.*, Vol. 78, 1973, p. 1.
11. ELIAS, J., *Calibration of Standard Stars for Planetary Reflectivity Studies*. Masters dissertation, M.I.T., Cambridge, Mass., 1972.
12. BURNS, R. G., *Electronic Spectra of Silicate Minerals: Application of Crystal-Field Theory to Aspects of Geochemistry*. Unpublished Ph.D. thesis, U. of Calif., Berkeley, Calif., 1965.
13. BURNS, R. G., *Mineralogical Applications of Crystal-Field Theory*, Cambridge U. Press, Cambridge, England, 1970.
14. WHITE, W. B., AND K. L. KEESTER, Optical Absorption Spectra of Iron in the Rock-Forming Silicates. *Am. Mineralogist*, Vol. 51, 1966, pp. 774–791.
15. WHITE, W. B., AND K. L. KEESTER, Selection Rules and Assignments for the Spectra of Ferrous Iron in Pyroxenes. *Am. Mineralogist*, Vol. 52, 1967, pp. 1508–1514.
16. BANCROFT, G. M., AND R. G. BURNS, Interpretation of the Electronic Spectra of Iron in Pyroxenes. *Am. Mineralogist*, Vol. 52, 1967, pp. 1278–1287.
17. ADAMS, J. B., AND A. L. FILICE, Spectral Reflectance 0.4 to 2.0 Microns of Silicate Rock Powders. *J. Geophys. Res.*, Vol. 72, 1967, pp. 5705–5715.
18. ADAMS, J. B., Lunar and Martian Surfaces: Petrologic Significance of Absorption Bands in the Near-Infrared. *Science*, Vol. 159, 1968, pp. 1453–1455.
19. HUNT, G. R., AND J. W. SALISBURY, Visible and Near-Infrared Spectra of Minerals and Rocks: I. Silicate Minerals. *Modern Geol.*, Vol. 1, 1970, pp. 283–300.
20. HUNT, G. R., AND J. W. SALISBURY, Visible and Near-Infrared Spectra of Minerals and Rocks: II. Carbonates. *Modern Geol.*, Vol. 2, 1971, pp. 23–30.
21. HUNT, G. R., J. W. SALISBURY, AND C. J. LENHOFF, Visible and Near-Infrared Spectra of Minerals and Rocks: III. Oxides and Hydroxides. *Modern Geol.*, Vol. 2, 1971, pp. 195–205.
22. HUNT, G. R., J. W. SALISBURY, AND C. J. LENHOFF, Visible and Near-Infrared Spectra of Minerals and Rocks: IV. Sulphides and Sulphates. *Modern Geol.*, Vol. 3, 1971, pp. 1–14.
23. HUNT, G. R., J. W. SALISBURY, AND C. J. LENHOFF, Visible and Near-Infrared Spectra of Minerals and Rocks: V. Halides, Phosphates, Arsenates, Vanadates and Borates. *Modern Geol.*, Vol. 3, 1972, pp. 121–132.
24. ADAMS, J. B., Uniqueness of Visible and Near-Infrared Diffuse Reflectance Spectra of Pyroxenes and Other Rock-Forming Minerals. In *Infrared and Raman Spectroscopy of Lunar and Terrestrial Minerals*, Kerr, ed., Academic Press, in press, 1974.
25. ADAMS, J. B., Visible and Near-Infrared Diffuse Reflectance Spectra of Pyroxenes as Applied to Remote Sensing of Solid Objects in the Solar System. *J. Geophys. Res.*, in press, 1974.
26. GAFFEY, M. J., *A Systematic Study of the Spectral Reflectivity Characteristics of the Meteorite Classes with Application to the Interpretation of Asteroid Spectra for Mineralogical and Petrological Information*, Ph.D. thesis, M.I.T., Cambridge, Mass., February 1974.
27. GAFFEY, M. J., *Spectral Reflectance Characteristics of the Meteorite Classes*, in preparation, 1974.
28. BURNS, R. G., AND D. J. VAUGHAN, Polarized Electronic Spectra. In *Infrared and Raman Spectroscopy of Lunar and Terrestrial Minerals*, Academic Press, in press, 1974.
29. BELL, P. M., H. K. MAO, AND G. R. ROSSMAN, Absorption Spectroscopy of Ionic and Molecular Units in Crystals and Glasses. In *Infrared and Raman Spectroscopy of Lunar and Terrestrial Minerals*, Kerr, ed., Academic Press, in press, 1974.
30. GAFFEY, M. J., AND R. G. BURNS, *The Angular Dependence of Photon-Electron Interaction in Transition Metal Silicates*, in preparation, 1974.
31. MCCORD, T. B., Color Differences on the Lunar Surface. *J. Geophys. Res.*, Vol. 74, 1969, p. 12.
32. MCCORD, T. B., AND T. V. JOHNSON, Spectral Lunar Reflectivity (0.30 to 2.50 Microns) and Implications for Remote Mineralogical Analysis. *Science*, Vol. 169, 1970, p. 855.
33. ADAMS, J. B., AND T. B. MCCORD, Remote Sensing of Lunar Surface Mineralogy; Implications From Visible and Near-Infrared Reflectivity of Apollo 11 Samples. In *Proc. Apollo 11 Lunar*

Science Conference, Vol. 3, A. A. Levinson, ed., 1970.

34. CONEL, J. E., Coloring of Synthetic and Natural Lunar Glass by Titanium and Iron. *Jet Propulsion Laboratory Space Programs Summary*, Vol. 3, 1970, pp. 26–31.
35. CONEL, J. E., AND D. B. NASH, Spectral Reflectance and Albedo of Apollo 11 Lunar Samples: Effects of Irradiation and Vitrification and Comparison with Telescopic Observations. *Proc. Apollo 11 Lunar Science Conference, Geochimica et Cosmochimica Acta*, Supplement 1, Vol. 3, 1970, pp. 2013–2023.
36. ADAMS, J. B., AND T. B. MCCORD, Optical Properties of Mineral Separates, Glass and Anorthositic Fragments from Apollo Mare Samples. In *Proc. Second Lunar Science Conference*, Vol. 3, A. A. Levinson, ed., 1971.
37. MAO, H. K., D. VIRGO, AND P. M. BELL, Sample 74220: Analysis of the Apollo 17 Orange Soil From Shorty Crater. *EOS, Trans. Am. Geophys. Union*, Vol. 54, 1973, pp. 598–599.
38. CHARETTE, M. P., T. B. MCCORD, C. PIETERS, AND J. B. ADAMS, Application of Remote Spectral Reflectance Measurements to Lunar Geology Classification and Determination of Titanium Content of Lunar Soils. *J. Geophys. Res.*, Vol. 79, 1974, p. 1239.
39. PIETERS, C., T. B. MCCORD, M. CHARETTE, AND J. B. ADAMS, Dark Mantling Material in the Apollo 17 Soil Samples. *Science*, Vol. 183, 1974, p. 1191.
40. ADAMS, J. B. AND T. B. MCCORD, Alteration of Lunar Optical Properties: Age and Composition Effects. *Science*, Vol. 171, 1971, p. 567.
41. ADAMS, J. B., AND T. B. MCCORD, Electronic Spectra of Pyroxene and Interpretation of Telescopic Reflectivity Curves of the Moon. In *Proc. Third Lunar Science Conference*, Vol. 3, D. R. Criswell, ed., 1972.
42. ADAMS, J. B. AND T. B. MCCORD, Vitrification Darkening in the Lunar Highlands and Identification of Descartes Material at the Apollo 16 Site. *Proc. Fourth Lunar Conference*, Vol. 1, 1973, p. 163.
43. DOLLFUS, A., Resultats Recents sur les Planetes Mercury, Venus et Mars Obtenus par les Observations Astronomiques au Sol. In *Moon and Planets*, Vol. II, A. Dollfus, ed., North-Holland Publishing Co., Amsterdam, 1967.
44. MCCORD, T. B., AND J. B. ADAMS, Mercury: Surface Composition From the Reflection Spectrum. *Science*, Vol. 178, 1972, p. 745.
45. MCCORD, T. B., AND J. B. ADAMS, Mercury: Interpretation of Optical Observations. *Icarus*, Vol. 17, 1972, p. 585.
46. MCCORD, T. B., AND J. B. ADAMS, The Spectral Reflectivity of Mars. *Science*, Vol. 163, 1969, p. 1058.
47. ADAMS, J. B., AND T. B. MCCORD, Mars: Interpretation of Spectral Reflectivity of Light and Dark Regions. *J. Geophys. Res.*, Vol. 74, 1969, pp. 4851–4856.
48. MCCORD, T. B., AND J. A. WESTPHAL, Mars: Narrowband Photometry 0.3 to 3.5 Microns of Surface Regions During the 1969 Apparition. *Ap. J.*, Vol. 168, 1971, pp. 143–153.
49. MCCORD, T. B., J. ELIAS, AND J. A. WESTPHAL, Mars: Spectral Albedo (0.3 to 2.5 Microns) of Small Bright and Dark Regions. *Icarus*, Vol. 14, 1971, pp. 245–251.
50. MCCORD, T. B., C. PIETERS, AND R. L. HUQUENIN, in preparation.
51. HANEL, R., B. CONRATH, W. HOVIS, V. KUNDE, P. LOWMAN, W. MAGUIRE, J. PEARL, J. PIRRAGLIA, C. PRABHAKARA, B. SCHLACHMAN, G. LEVIN, P. STRAAT, AND T. BURKE, Investigation of the Martian Environment by Infrared Spectroscopy on Mariner 9. *Icarus*, Vol. 17, 1972, p. 423.
52. HUNT, G. R., L. M. LOGAN, AND J. W. SALISBURY, Mars: Components of Infrared Spectra and the Composition of the Dust Cloud. *Icarus*. Vol. 18, 1973, p. 459.
53. HOUCK, J. R., J. B. POLLACK, C. SAGAN, D. SCHAACK, AND J. A. DECKER, JR., High Altitude Infrared Spectroscopic Evidence for Bound Water on Mars. *Icarus*, Vol. 18, 1973, p. 470.
54. HUGUENIN, R. L., T. B. MCCORD, AND J. B. ADAMS, in preparation.
55. HUGUENIN, R. L., Photo-Stimulated Oxidation of the Martian Surfaces. *J. Geophys. Res.*, in press, 1974.
56. HUGUENIN, R. L., Photo-Stimulated Oxidation of Magnetite: 1. Kinetics and Alteration Phase Identification. *J. Geophys. Res.*, Vol. 78, 1973, p. 8481.
57. HUGUENIN, R. L., Photo-Stimulated Oxidation of Magnetite: 2. Mechanism. *J. Geophys. Res.*, Vol. 78, 1973, p. 8495.
58. SANDAKOVA, E. V., Concerning Color Indices of Minor Planets. *Astron. Circ.*, Acad. Sci. U.S.S.R., 1955, p. 163.
59. SANDAKOVA, E. V., Interpretation of Color Indices of Minor Planets. *Pub. Kiev Univ. Astron. Obs.*, Vol. 8, 1959.
60. SANDAKOVA, E. V., Concerning the Color Indices of Minor Planets. *Pub. Kiev Univ. Astron. Obs.*, Vol. 10, 1962.
61. WATSON, F. G., *Small Bodies and the Origin of the Solar System*. Ph.D. dissertation, Harvard University, Cambridge, Mass., 1938.
62. KITAMURA, M., A Photoelectric Study of Colors of Asteroids and Meteorites. *Pub. Astron. Soc. Japan*, Vol. 11, 1959, pp. 79–89.
63. CHAPMAN, C. R., T. B. MCCORD, AND C. PIETERS, Spectrophotometric Study of the Composition of (1685) Toro. *Astron. J.*, Vol. 78, 1973, p. 502.

64. McCord, T. B., and C. R. Chapman, Asteroid Spectral Reflectivities: II. To be submitted to *Astro. Phys. J.*, 1973.
65. Hunt, G. R., and J. W. Salisbury, Visible and Near-Infrared Spectra of Minerals and Rocks: VIII. Meteorites. In preparation, 1974.
66. Chapman, C. R., and J. W. Salisbury, Comparison of Meteorite and Asteroid Spectral Reflectivities. *Icarus*, Vol. 19, 1973, p. 507.
67. Johnson, T. V., and F. P. Fanale, Optical Properties of Carbonaceous Chondrites and Their Relationship to Asteroids. *J. Geophys. Res.*, Vol. 78, 1973, p. 8507.
68. McCord, T. B., and M. J. Gaffey, Asteroids: Surface Composition Using Reflection Spectroscopy. Submitted to *Science*, 1974.
69. Johnson, T. V., and T. B. McCord, Galilean Satellites: The Spectral Reflectivity 0.30–1.10 Micron. *Icarus*, Vol. 13, 1970, pp. 37–42.
70. Johnson, T. V., Galilean Satellites: Narrowband Photometry 0.30 to 1.10 Microns. *Icarus*, Vol. 14, 1971, p. 94.
71. Johnson, T. V., and T. B. McCord, Spectral Albedo of the Galilean Satellites—0.3–2.5 Microns. *Ap. J.*, Vol. 169, 1971, pp. 589-594.
72. Pilcher, C. B., S. T. Ridgeway, and T. B. McCord, Galilean Satellites: Identification of Water Frost. *Science*, Vol. 178, 1972, p. 1087.
73. Lebofsky, L. A., *Chemical Composition of Saturn's Rings and Icy Satellites*. Ph.D. dissertation, M.I.T., Cambridge, Mass., 1973.
74. Lewis, J. S., Low Temperature Condensation From the Solar Nebula. *Icarus*, Vol. 16, 1971, pp. 241–252.
75. Lewis, J. S., Origin and Composition of the Terrestrial Planets and Satellites of the Outer Planets. In *Origin of the Solar System*, C.N.R.S., Paris, France, 1973.
76. McCord, T. B., T. V. Johnson, and J. Elias, Saturn's Satellites: Narrowband Spectral Photometry (0.3 to 1.1 microns). *Ap. J.*, Vol. 165, 1971, pp. 413–424.
77. Lebofsky, L. S., T. V. Johnson, and T. B. McCord, Saturn's Rings: Spectral Reflectivity and Compositional Implications. *Icarus*, Vol. 13, 1970, pp. 226–230.
78. Franklin, F. A., and A. F. Cook, Optical Properties of Saturn's Rings II: Two-Color Phase Curves of the Two Bright Rings. *Astron. J.*, Vol. 70, 1965, pp. 704–720.
79. Cruikshank, D. P., Paper presented at International Astronomical Union, 40th Symposium, Marfa, Texas, October 1969.
80. Pilcher, C. B., C. R. Chapman, L. A. Lebofsky, and H. Kieffer, Saturn's Rings: Identification of Water Frost. *Science*, Vol. 167, 1970, pp. 1372–1373.